HAVSTOVAN
FAROE MARINE RESEARCH INSTITUTE

Bottom temperature
and echo-sounder corrections around the Faroe Plateau

Tórshavn · May 2018

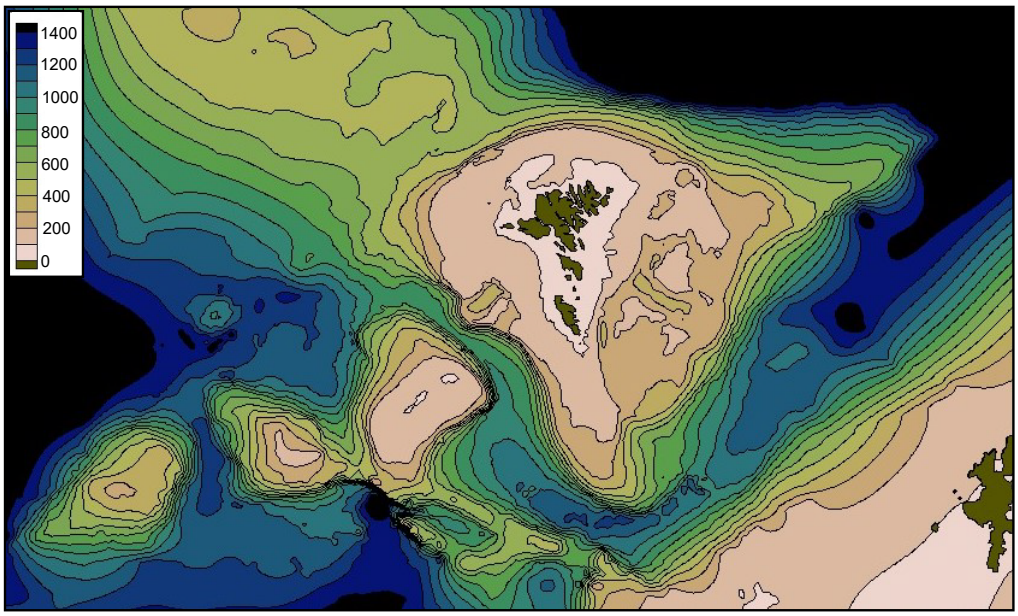

Map: Knud Simonsen

Bogi Hansen

HAVSTOVAN NR.: 18-02
TECHNICAL REPORT

Bottom temperature

and echo-sounder corrections around the Faroe Plateau

Bogi Hansen

Abstract

This report describes the main features of the bottom temperature in the ocean area around the Faroe Islands with a special focus on the Faroe Plateau and Faroe Bank, which have huge importance for the demersal fisheries. The report also includes a section on how to correct echo-sounder depths for sound speed variations in different parts of the region.

1 Introduction

The Faroe Plateau is surrounded by fairly deep waters on almost all sides with the Norwegian Sea towards the Northeast and the Iceland Basin towards the West (Figure 1). The Iceland-Faroe Ridge, which has a sill depth of almost 500 m, reaches towards the Northeast. The Faroe-Shetland Channel separates the Faroe Plateau from the Scottish Shelf and the Faroe Bank Channel separates it from the Faroe Bank.

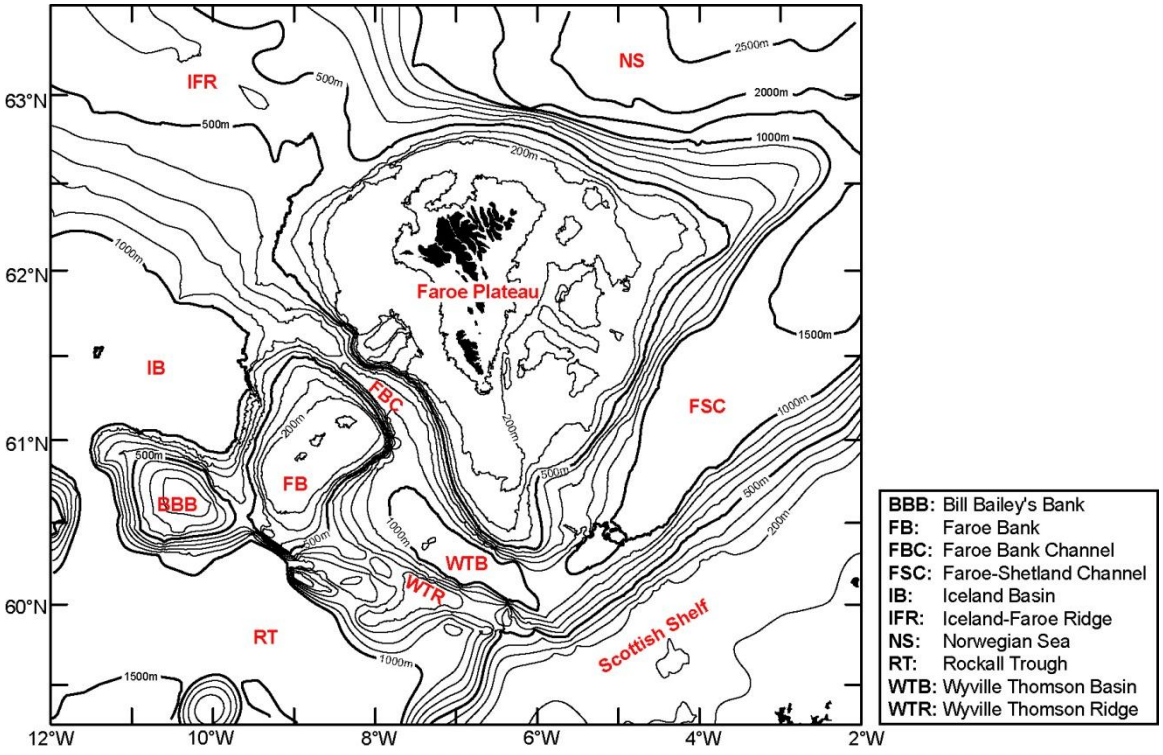

Figure 1. Bottom topography around the Faroe Plateau. For regions shallower than 1000 m, isobaths are plotted for every 100 m with the 500 m isobath thicker than the others. Deeper than 1000 m, the isobath interval is 500 m.

In the upper layers, the temperature and water mass composition around the Faroe Plateau are determined by the confluence of two major current systems: The North Atlantic Current bringing warm (and saline) ***Atlantic Water*** and the East Icelandic Current, which carries colder (and less saline) ***Arctic Water*** into the region (Figure 2a).

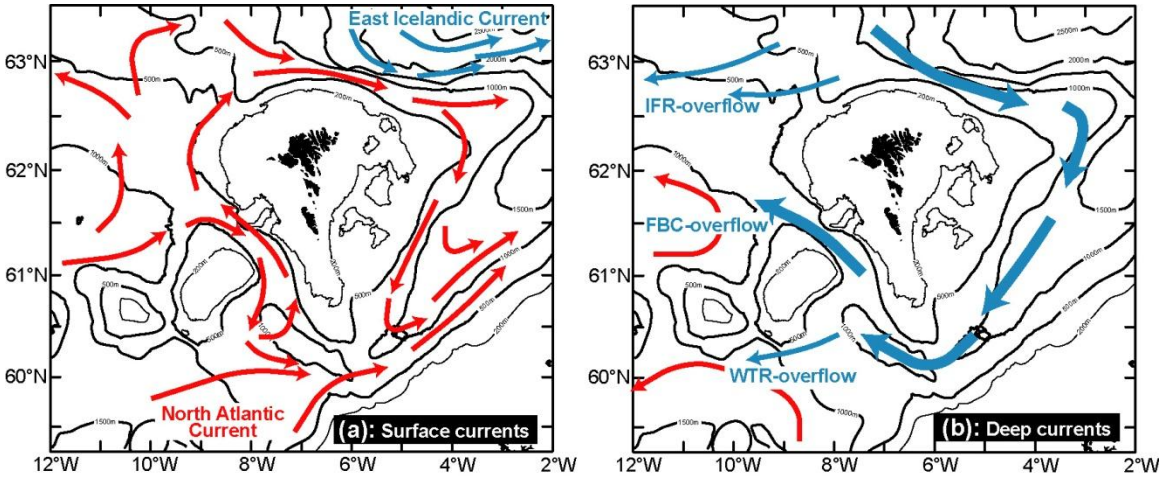

Figure 2. Main current systems in the upper layer **(a)** and at depth **(b)**. Red arrows: warm water. Blue arrows: cold water.

In the deeper layers, there are also two confluent current systems (Figure 2b). One of them is again the Atlantic water coming from the Southwest. At depth, it is not as warm as close to the surface, but it is still fairly warm down to large depths. Its northeastward progression is blocked by the Wyville Thomson Ridge and the Iceland-Faroe Ridge giving rise to two cyclonic gyres, one in the Rockall Trough, and one in the Iceland Basin.

The other deep current system is linked to the overflow of cold water from the Norwegian Sea into the Atlantic. This ***Deep Water*** is a cold and dense water mass formed by atmospheric cooling and sinking farther north in the Arctic Mediterranean. It fills the depths of the Norwegian Sea, up to the sill level of the Iceland-Faroe Ridge where some of it passes the ridge as ***IFR-overflow***. By far most of the Deep Water in the Norwegian Sea escapes by another route, however, flowing southwestwards into the Faroe-Shetland Channel. From there, a small part flows over the WTR, but most of this water continues through the Faroe Bank Channel to become ***FBC-overflow*** (Figure 2b).

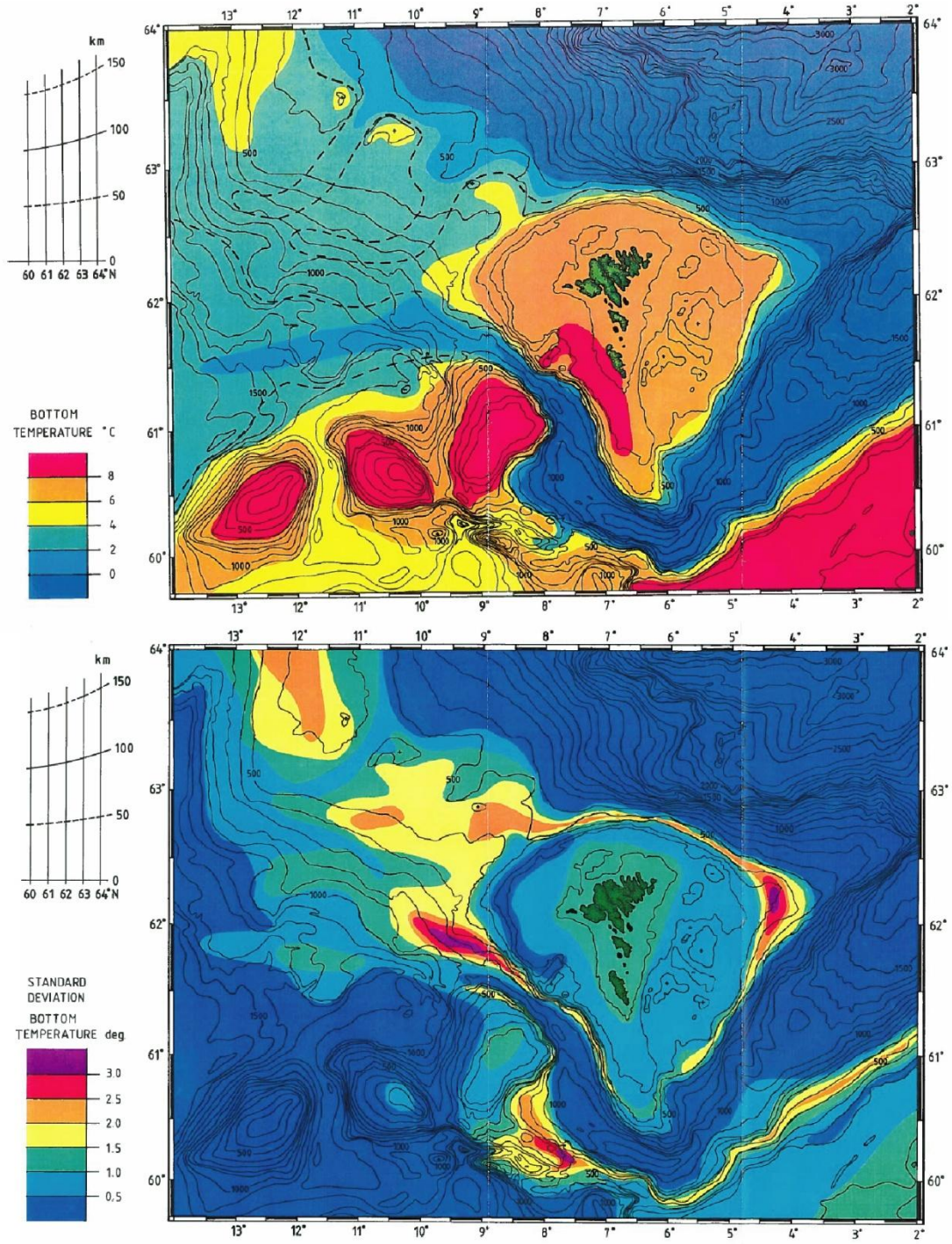

Figure 3. Bottom temperature map produced by Håkan Westerberg in 1990 (Westerberg, 1990) showing average (top panel) and standard deviation (bottom panel).

The East Icelandic Current is turned away before it reaches the Faroe Plateau and its water does not affect bottom temperatures in the Faroe region to any significant degree. The bottom temperature at any given location is therefore given by the relative influences that the Atlantic Water and the Deep Water have on the location. A location that is permanently covered by Atlantic Water will have a relatively stable high bottom temperature, although decreasing with depth. Regions that are permanently covered by Deep Water will similarly have stable low temperatures. Intermediate temperatures are found in regions where the two water masses meet and, since the boundary between them moves continually, these locations also tend to have highly variable bottom temperatures.

This general principle explains most of the features in Figure 3, which is an illustration of the bottom temperature in the Faroe region showing both its average and its standard deviation. The figure was produced by Håkan Westerberg in 1990 within the BIOFAR project (Westerberg, 1990).

In this report, we will update Figure 3. As to its large scale features, little can be added or amended, but new observations can add some details and refine some of the features. The observational data set includes both CTD observations from Faroese research vessels and measurements from self-recording instruments that have been deployed on or close to the bottom over prolonged periods. This allows us not only to consider average values, but also the variations and to check whether there are systematic temporal variations: long-term changes, seasonal variations, or variations following the tidal cycle. We also include some results from published literature.

The bottom temperature at a given location may be a critical parameter for the living conditions of many fish species and one of the motivations for this report was inquiries from Faroese fishermen on more detailed information on the bottom temperature. The main focus of the report is therefore on the Faroe Plateau proper since it is an important area for Faroese demersal fisheries and has been more intensively observed than the surrounding areas. The shallowest part of the Faroe Plateau is strongly affected by air-sea heat exchange and forms a partly closed system, which has been described elsewhere (e.g., Larsen, 2008; 2009). Here, the area inside the 100 m depth contour on the Faroe Plateau is therefore to a large extent ignored.

The report is structured such that the data from deployed instruments and CTD data are discussed separately in Sect. 2 and Sect. 3, respectively. This is followed by Sect. 4, which documents results from trawl-attached temperature loggers and Sect. 4 reporting bottom temperatures from Seagliders. The results from the different data sets are then synthesized in Sect. 6. In addition to bottom temperature, the comprehensive CTD data set also allows an investigation of the typical sound speed variations in the region, which may be used to correct echo-sounder depth measurements. This is discussed in Sect. 7. The report ends with a reference list and two appendices containing some of the most voluminous tables as well as information on statistical methods.

2 Bottom temperature measurements from moored instruments

Since the mid-1990s, instruments that measure temperature at or very close (< 10 m) to the bottom have been deployed at 14 sites on the Faroe Plateau or the southernmost part of the Iceland-Faroe Ridge (Figure 4 and Table 1). At some sites, there have been more than one deployment and Table A1 gives a more detailed list of all the deployments. The bottom depth ranges from 185 m to 986 m.

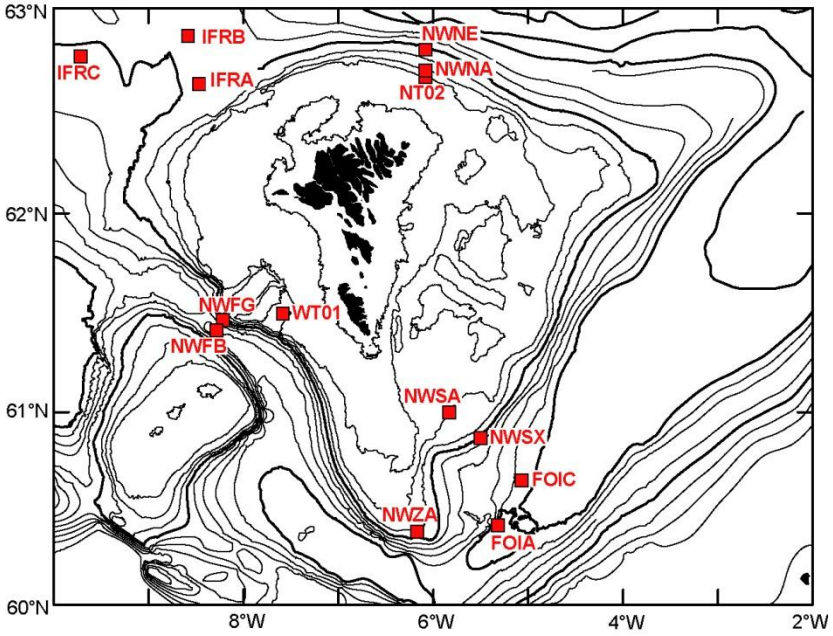

Figure 4. Sites where instruments with continuous bottom temperature measurements have been deployed.

As indicated in Table A1, four types of instrument have been used: RDI ADCPs (Acoustic Doppler Current Profilers), SeaBird Microcats (SBE37), Aanderaa RCM current meters, and specially developed bottom temperature loggers (BTLs) that are placed on the bottom and may be interrogated acoustically. All of these instruments have accuracies well exceeding our requirement (0.01°C) except for the ADCPs, which may have biases well above this limit. These biases seem, however, to be fairly constant in time for each instrument. As long as we are mainly interested in temperature variations and from the same instrument, the bias should not be too critical, but this has to be kept in mind.

Table 1. List of sites at which continuous bottom temperature measurements have been recorded. "Botm" is bottom depth (in m). "Number" is total number of temperature measurements at the site. "Days" is total number of days. The last four columns list average, standard deviation, minimum, and maximum of individual bottom temperature measurements at the site.

Site	Location		Botm	Period	Number	Days	Tavg	Tstd	Tmin	Tmax
NT02	62°40'N	6°05'W	185	20151015-20170831	16454	685	7.99	0.64	3.47	9.73
WT01	61°30'N	7°35'W	243	20151017-20170902	16475	685	7.79	0.57	6.13	9.45
NWSA	61°00'N	5°50'W	295	19951110-20000620	84705	1107	7.04	0.78	3.18	8.45
NWNA	62°42'N	6°05'W	300	19960124-20150525	484059	6663	7.85	0.80	0.27	9.82
NWZA	60°23'N	6°10'W	416	20110611-20140517	49423	684	4.70	1.65	0.05	9.28
NWNE	62°48'N	6°05'W	455	20000706-20150905	267684	3852	3.15	1.90	-0.86	8.13
IFRA	62°38´N	8°28´W	497	20030704-20050524	112781	584	2.69	2.04	-0.44	7.97
IFRB	62°52'N	8°35'W	495	20030704-20040611	24709	342	1.77	1.55	-0.61	6.60
IFRC	62°46'N	9°43'W	497	20040703-20050524	23406	324	1.98	1.42	-0.45	5.50
NWSX	60°52´N	5°30´W	550	20090606-20130519	99643	1037	0.98	1.05	-0.58	7.70
NWFG	61°28'N	8°13'W	561	20080516-20090516	26272	364	3.76	1.25	0.31	8.32
NWFB	61°25'N	8°17'W	814	20010708-20170518	729606	5318	-0.39	0.15	-0.77	0.56
FOIC	60°39'N	5°04'W	910	20010707-20020616	8238	343	-0.71	0.08	-0.87	-0.31
FOIA	60°25'N	5°19'W	986	20010707-20020616	8237	343	-0.74	0.05	-0.85	-0.47
					1951692	22331				

2.1 Long-term variation

Figure 5 shows 3-year running mean bottom temperature at three sites that have been occupied over more than 10 years together with the temperature at the core of the Atlantic water reaching the Faroe Plateau from the West (Larsen et al., 2012). At site NWNA (Figure 5a), the bottom temperature variation has been very similar to the variation in the Atlantic water, although approximately 1°C colder. At the deeper site, NWNE (green curve in Figure 5a), the similarity is much less evident. At the deep site, NWFB (Figure 5b), there has been a fairly steady warming since the beginning of the 21st century, although considerably weaker than the variations seen in the upper layers.

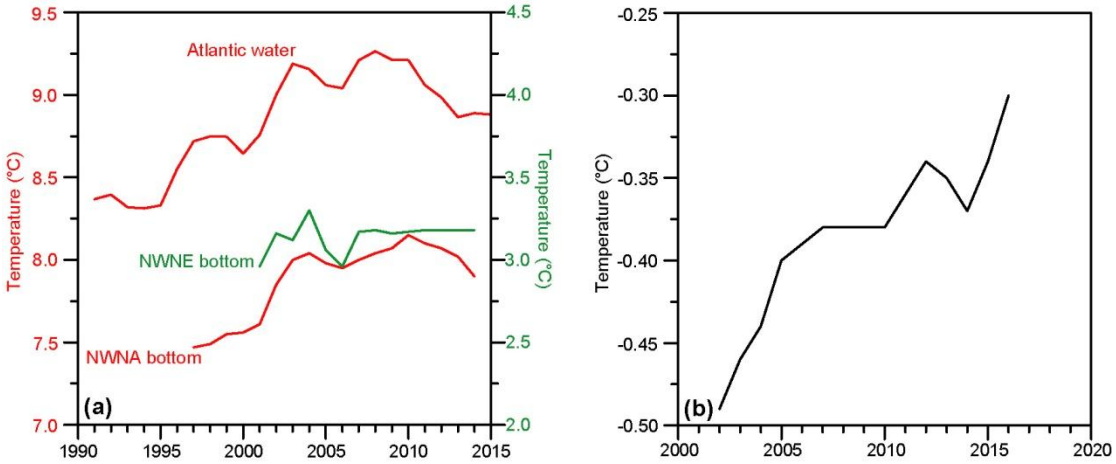

Figure 5. Long-term (3-year running mean) temperature variation. **(a)** Red curves: temperature of the Atlantic core in the Faroe Bank Channel and bottom temperature at ADCP site NWNA, left hand y-axis. Green curve: Bottom temperature at ADCP site NWNE, right hand y-axis. **(b)** Bottom temperature at ADCP site NWFB. Note that there is a factor 10 difference between the temperature scales in (a) and (b).

2.2 Seasonal variation

The seasonal bottom temperature variation at the deployment sites is illustrated in Figure 6. The four shallowest sites (NT02, WT01, NWSA, NWNA) all exhibit similar variations, along expected lines with the coldest month in spring – typically March – and the warmest in late autumn – typically November. The seasonal range is also similar for these four sites with the increase from coldest to warmest month slightly more than 1°C.

Almost the opposite seasonal variation is shown by several of the deep sites. This is most clearly seen at site NWFB at the bottom of the Faroe Bank Channel where it has been noted before (Hansen and Østerhus, 2007) and associated with the seasonality of the overflow volume transport. At intermediate depths, the seasonal variation in bottom temperature is less systematic and seems often to be dominated by other types of variability, e.g. at site NWNE.

Table 2. Correlation coefficients (R) between the tidal temperature anomaly, T_i', and the tidal speed, C_i' for the ADCP sites. The correlations are calculated for the deepest bin, close to bottom, as well as for a more shallow bin, for which there still are 80% good data on average. Only days with 80% good data are included and the number of these is listed (Numb). Also listed are overall averages of T_i' (in °C)and C_i' (in cm s^{-1}). Asterisks indicate statistical significance (Appendix B).

	Deepest bin					Top bin					
Site	Depth	Numb	$<C_i'>$	$<T_i'>$	R	Bin	Depth	Numb	$<C_i'>$	$<T_i'>$	R
NWSA	279	1053	19.	0.093	0.089*	18	109	885	25.	0.086	0.060
NWNA	282	5865	17.	0.207	0.199***	17	122	5039	19.	0.198	0.086***
NWZA	397	684	31.	0.767	0.444***	35	57	487	28.	0.764	0.122
NWNE	425	2678	19.	0.811	0.315***	11	175	2133	16.	0.781	-0.025
IFRA	480	259	23.	0.373	0.032	43	60	175	28.	0.310	-0.032
IFRB	475	342	19.	0.269	0.242***	43	55	265	34.	0.251	-0.004
IFRC	479	324	19.	0.297	0.128*	43	59	231	30.	0.279	0.037
NWSX	528	693	24.	0.544	0.483***	45	88	476	19.	0.486	0.052
NWFG	542	364	17.	0.781	0.207***	46	92	240	19.	0.791	0.361***

2.3 Tidal variations

In order to look for a possible tidal effect on the bottom temperature, we define the temperature deviation $\Delta T_i(t)$ at a specific time t during day i as the deviation from the average for the same day: $\Delta T_i(t) = T_i(t) - <T_i>$. In a similar manner, we define the two components of the tidal current, $\Delta U_i(t)$ and $\Delta V_i(t)$, as the deviations of the instantaneous velocity from the

daily averages. The temperature anomaly for day i, T_i', may then be defined as the root-mean-square value of $\Delta T_i(t)$ while the tidal speed for day i, C_i', is the square root of the daily average of $(\Delta U_i(t))^2+(\Delta V_i(t))^2$.

If there is a strong tidal effect on the bottom temperature, we might expect a high correlation between these two parameters and at some sites, we do see (Table 2) fairly high correlation coefficients when T_i' is correlated with C_i' for the deepest bin (bin 1). As expected, the correlation coefficients are generally lower when we go higher in the water column and, in most cases they are so low that one would not expect any useful relationships.

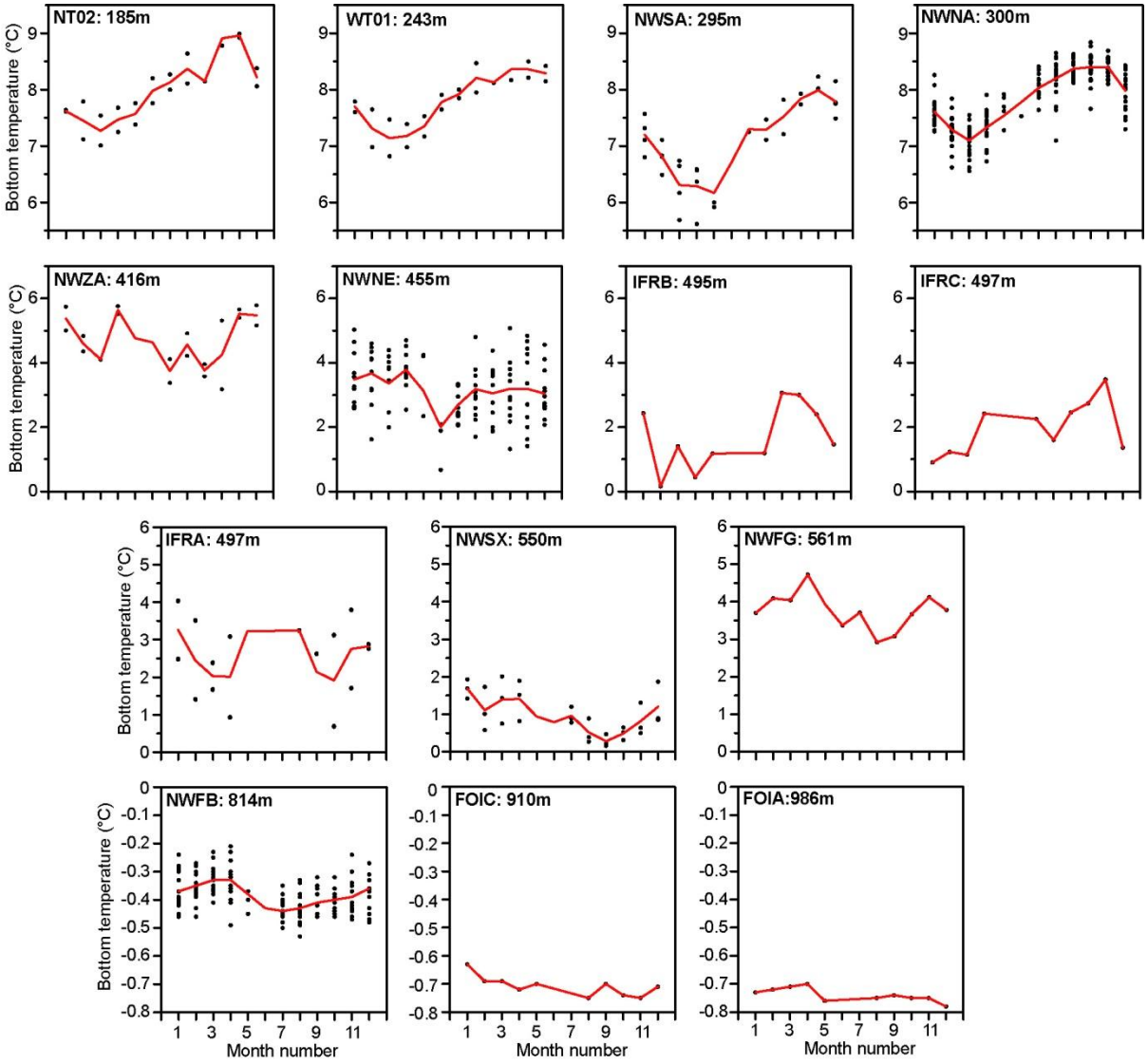

Figure 6. Seasonal variation of the bottom temperature at the deployment sites. Individual dots are for one month. The red line shows monthly averages for the whole record.

In spite of the low correlations in Table 2, it appears that several of the sites do have a fairly consistent relationship between tidal current direction and temperature (Figure 7). To produce this figure, we determined for each day, the direction of the tidal current ($\Delta U_i(t)$, $\Delta V_i(t)$) at the time that the bottom water was warmest (red bars) and coldest (blue bars). Figure 7 then shows the frequency distributions for these directions for most of the ADCP sites (not the deepest ones). For this to be useful, the red bars and the blue bars should be clearly separated, preferably with a difference of 180°.

From this criterion, the only sites where the tidal current direction for bin 1 gives a clear indication of the bottom temperature anomaly are NWNA, NWZA, NWNE, NWSX, and NWFG. The inclination of the M2 tidal ellipse at each site (Table A1) is indicated by a black arrow in Figure 7 where we have chosen the direction (180° ambiguity) that has the Faroe Plateau on the right hand side. For NWNA, NWZA, NWNE, and NWSX, the warmest bottom water generally occurs when the tidal current goes in this direction. This pattern will be further discussed in Sect. 4.3.

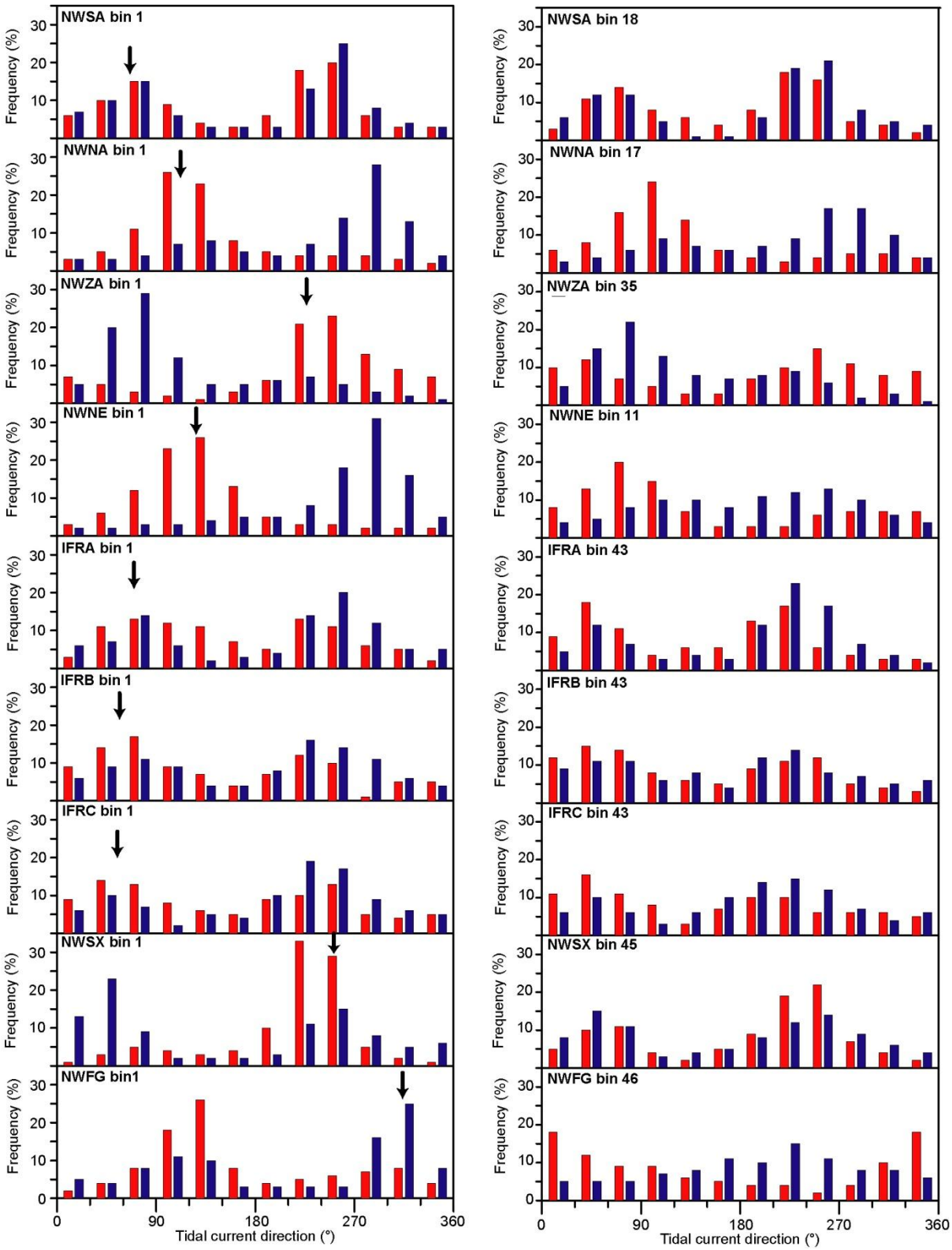

Figure 7. Frequency distribution of the tidal current direction (in 30° bins) for the warmest (red bars) measurements each day for the deepest bin (left hand panels) and for the topmost bin with at least 80% good data (right hand panels). Days with average tidal current C_i' weaker than 10 cm s^{-1} were ignored. Black arrows in the left hand panels indicate the inclination (from Table A1) of the M2 tidal ellipse with the Faroe Plateau on the right hand side.

The main purpose of Figure 7 was to see if there was a clear relationship between bottom temperature and the tidal current close to the surface, since this might be used for practical purposes during fisheries. That possibility is explored in the right hand panels of Figure 7 where the tidal current is from the uppermost bin with relatively good data, rather than

bin 1. It appears that for some of the sites – especially the shallow ones – the same relationship holds for the near-surface tidal current as for bin 1.

Thus, there is some evidence supporting the general relationship that the bottom temperature is highest when the tidal current goes along the bottom topography with the shallow water on the right hand side. This is what one would expect with an anticyclonically rotating tidal current as long as the bottom temperature decreases in the off-shelf direction. That will generally be the case for sites on the slope such as NWNA, NWNE, NWSX, and NWZA. Although fairly deep, site NWSA is on a rather flat part of the Faroe Plateau (Figure 4), where this condition is not necessarily fulfilled. Similar arguments may be used for the three sites on the Iceland-Faroe Ridge (IFRA, IFRB, IFRC), which perhaps may explain the appearance of these four sites in the left hand panels of Figure 7. For this relationship also to be applicable to near-surface tidal currents, the tidal current has to be fairly barotropic, which is generally only the case for the shallower ADCP sites, which may go a long way to explain the right hand panels of Figure 7.

2.4 Extension of intermediate depth bottom temperature series

To map the boundary between the Atlantic Water and the Deep Water adequately, we especially need measurements from intermediate depths. In addition to the long-term site NWNE, there are two other deployment sites at intermediate depths, close to the boundary. These are NWZA and NWFG, but they are unfortunately rather short, only 684 and 364 days, respectively, while at the same time highly variable (Table 1). The question therefore arises whether they can be extended by relating them to some other long-term time series.

For NWZA, the obvious time series to compare with would be satellite altimetry and daily bottom temperature at NWZA was correlated with various combinations of altimetry grid points from the AVISO+ (http://www.aviso.altimetry.fr) data set. The highest correlation coefficient (R = 0.43) was found when correlating with the difference in sea level anomaly (SLA) between a grid point at (61.125°N, 6.625°W) and one at (60.375°N, 6.125°W). Thus, the warmest bottom water is found when the surface velocity towards the east is strong. This is a reasonable result, since it indicates a deep Atlantic water layer (Hansen et al., 2017). The bottom temperature at NWZA was then regressed on this series (standard linear regression) and the regression equation was used to estimate the average bottom temperature at NWZA for the period from 1 Jan 1993 to 31 Dec 2014, for which we have altimetry data. The result was almost identical to the average value during the deployment period.

A similar procedure was attempted for NWFG, but the highest correlation coefficient with SLA differences was only R = 0.16 and not statistically significant. Instead, daily values of the bottom temperature at NWFG were correlated with various characteristics of the daily averaged velocity profile at site NWFB (Figure 4), which is close to NWFG. Here, the highest correlation coefficient (R = 0.41) was found with the depth of the interface between cold Deep Water and the warm Atlantic Water, as determined from the velocity profile (Hansen and Østerhus, 2007). Again, this is a reasonable result. The time series at NWFB are much longer than at NWFG, 7104 days compared to 364. A regression analysis was therefore used to extend the average bottom temperature at NWFG but, again, the difference was marginal (0.09°C).

Although higly significant ($p < 0.001$ taking into account serial correlation), the correlation coefficients in both these cases were below 0.5 and so the regressions explain less than 25% of the variances. Nevertheless, the results indicate that the deployments have not been made during exceptional conditions and that the values for NWZA and NWFG in Table 1 may be representative for longer periods.

3 Bottom temperature from CTD profiles

From the CTD dataset at Havstovan, we selected all stations within the geographical region: 59.25°N - 63.5°N, 12°W - 2°W for which the profile reached at least 100 m in depth excluding stations shallower than 1000 m on the Scottish side of the Faroe-Shetland Channel. This was a total of 8911 CTD stations. Using the sound velocity profiles calculated from the CTD data, corrected bottom depths were calculated for each station and the minimum distance of the CTD from the corrected bottom (ΔD) determined. To get an impression of the temperature gradient close to the bottom, we also determined the temperature difference (ΔT) between the deepest CTD value and the value that was ΔD higher in the water column. We then excluded stations shallower than 800 m for which ΔD > 30 m or ΔT > 0.5°C. This reduced the selected dataset to 7389 CTD stations (Figure 8).

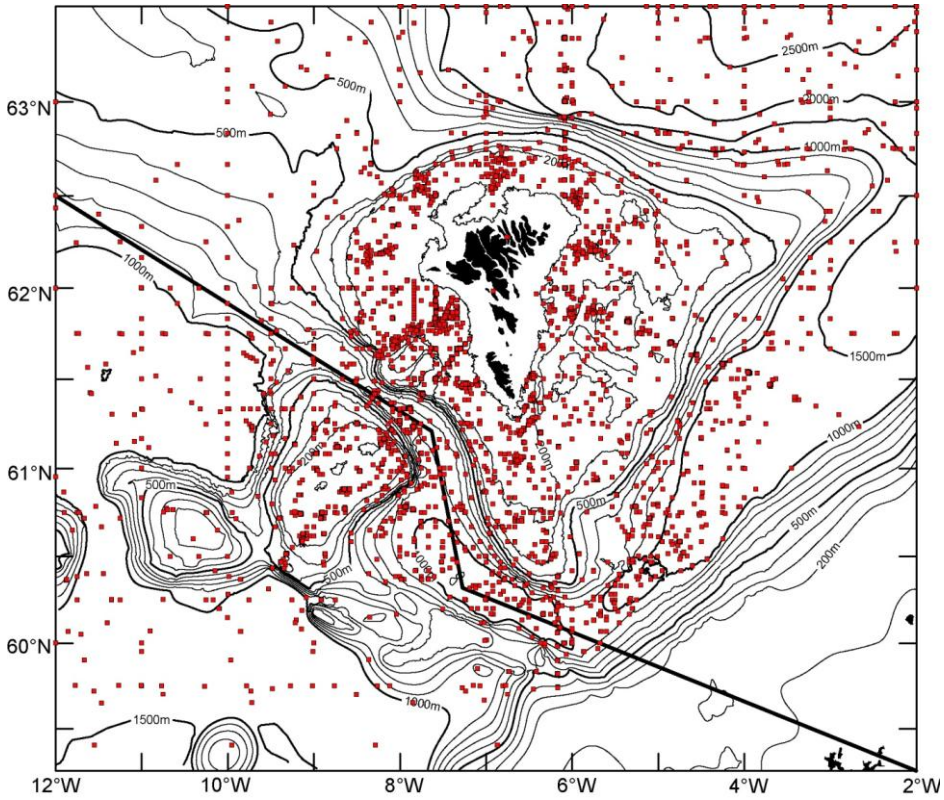

Figure 8. Locations of the 7389 selected CTD stations. The thick black line divides the area into the Southwestern region and the Northeastern region.

Within this area, there are considerable differences in water mass conditions. We therefore divide the area into two regions: the Southwestern region and the Northeastern region. For stations shallower than 800 m, the restriction that ΔD ≤ 30 m and ΔT ≤ 0.5°C should ensure that the deepest CTD observation normally will be close to the bottom temperature. For deeper stations, we require that the CTD reaches at least down to 750 m. In the Northeastern region surrounding the Faroe Plateau (Figure 8), this should ensure that the temperature is close to its coldest value.

In the Southwestern region, we require additionally that the deepest CTD observation is no more than 75 m from the corrected bottom depth. Over most of that region, this should give a good estimate of the bottom temperature although it will always be an overestimate. In areas with permanent or intermittent overflow close to the bottom, the temperature may still decrease substantially within the deepest 75 m layer. This is especially the case for the part of the Iceland Basin that is affected by the overflow plume from the Faroe Bank Channel. This will be treated separately.

In order to separate geographical and depth variations, the two regions were further subdivided. The Northeastern region was divided into four subregions as indicated in Figure 9 whereas the Southwestern region was divided into three subregions. In Figure 10, we have then plotted bottom temperature as a function of depth for each region where the colours of the dots indicate the subregions.

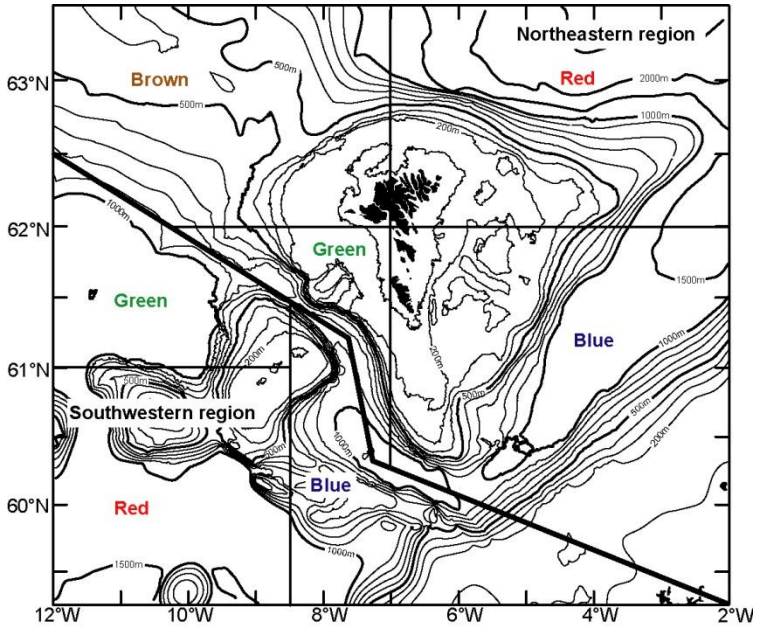

Figure 9. Subdivision of the two regions. The colour indications refer to the colours of the dots in Figure 10.

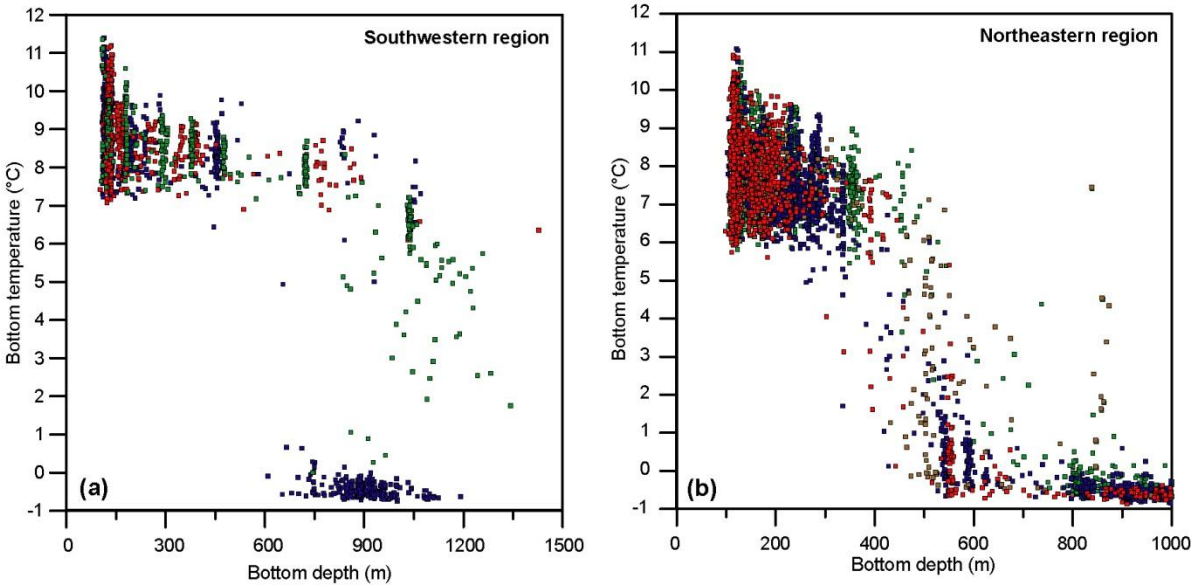

Figure 10. Bottom temperature as a function of depth for the Southwestern region **(a)** and for the Northeastern region **(b)**. The different colours refer to the subregions as indicated in Figure 9.

3.1 CTD observations from standard sections

We now will use CTD observations from standard stations, combined with bottom temperature measurements at long-term deployment sites, where possible. The standard stations are along 5 standard sections, shown in Figure 11.

The most comprehensive data is from section N along the 6°05'W meridian where there are two deployment sites on the bottom: NWNA at 300 m depth and NWNE at 455 m depth and 14 standard stations N01 to N14. One of these stations, N04 at latitude 62°20'N, is located over the deep part of the slope (bottom depth ≈ 550 m) and we may compare temperature measurements from individual CTD occupations of N04 with simultaneous bottom temperature measurements at the two deployment sites. The result is shown in Figure 12 where we see that the depth at which the temperature at N04 is equal to the bottom temperatures at the deployment sites may vary considerably.

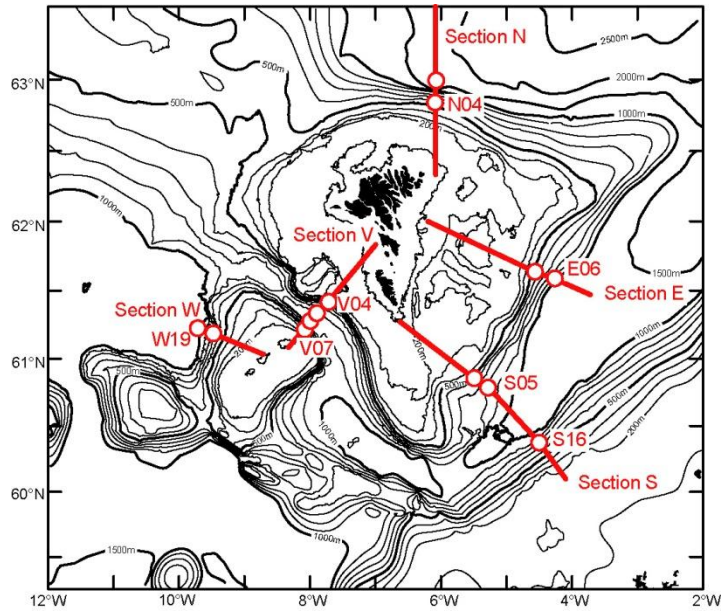

Figure 11. Map of standard sections (red lines) with standard stations that are used to determine bottom temperature indicated by red circles.

Figure 12 does not look very encouraging, but it may still be worthwhile to compare average conditions, which is done in Figure 13. The right hand panel of that figure shows the average temperature profiles of N04 based on 90 occupations and of N05 based on 87 occupations. From these, average isotherm depths have been extracted and plotted in the left hand panel of Figure 13 together with the average bottom temperatures at the two deployment sites. The thin red lines in this figure show that the two sets of measurements are quite consistent so that we can extrapolate the isotherm depths at N04 onto the slope bottom to determine the average bottom depths for the various isotherms on section N (Table 3). We only consider isotherms ≤ 6°C because the warmer water varies considerably in temperature both seasonally and inter-annually (Figure 5 and Figure 6). The CTD data in Figure 13 are from the period 1996-2015 in order to be comparable to the deployment periods, but for Table 3, there is a longer period, more comparable to sections E and V.

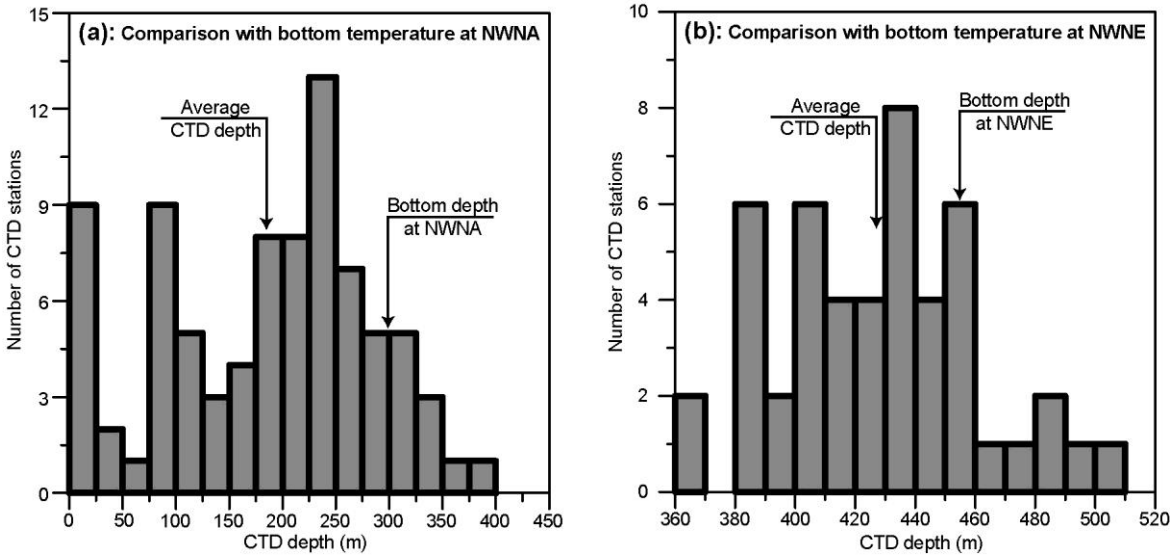

Figure 12. Frequency distributions of the depths at which CTD profiles from standard station N04 have the same temperature simultaneously (within one hour) as the bottom temperature at site NWNA **(a)** and NWNE **(b)**. In (a), the shallowest bin (0 to 25 m) includes occasions when the whole water column at N04 was colder than the bottom temperature at NWNA.

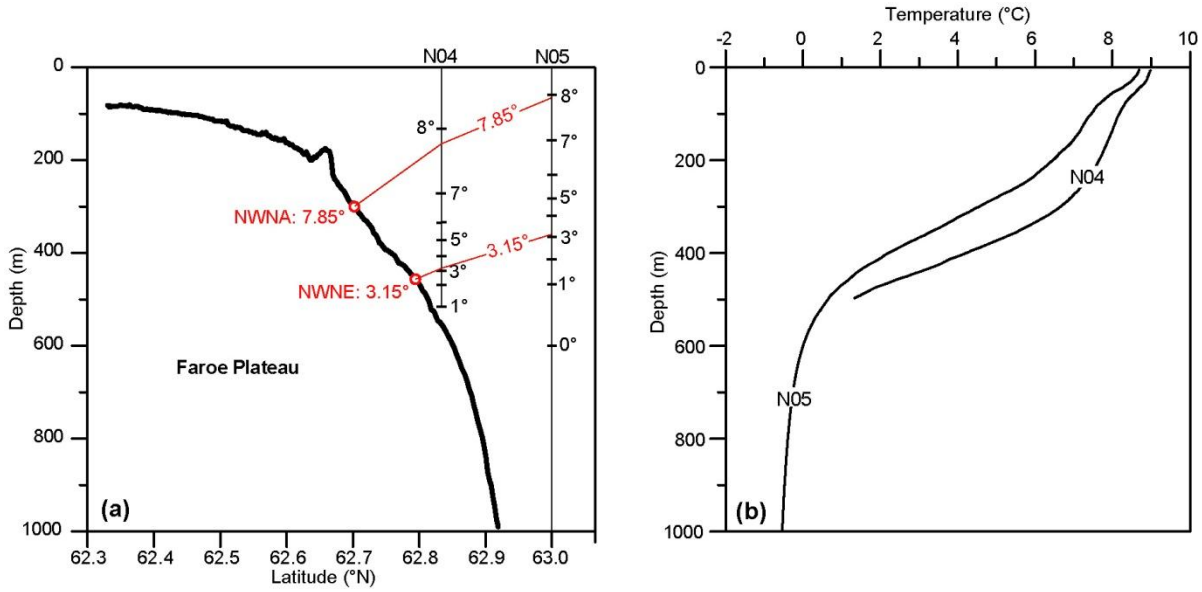

Figure 13. Temperature along section N. **(a)**: Average isotherm depths at standard CTD stations N04 and N05 and average bottom temperature at deployment sites NWNA and NWNE. Thin red lines show the depths of the two isotherms representing the average bottom temperatures at the two sites. **(b)**: Average temperature profiles at standard CTD stations N04 (90 occupations) and N05 (87 occupations) in the period 1996-2015.

Table 3. Estimated depths of isotherms where they hit the slope bottom on various standard sections either on the Faroe Plateau side or on the Scottish side of the Faroe-Shetland Channel or the Faroe Bank slope.

Section	Slope	Period	6°C	5°C	4°C	3°C	2°C	1°C
N	Faroe Plateau	1988-2016	369m	403m	428m	460m	481m	520m
E	Faroe Plateau	1989-2015	347m	371m	406m	435m	464m	520m
S	Faroe Plateau	1994-2015	351m	390m	420m	448m	480m	518m
S	Scottish	2012-2016	>491m	>532m	>570m	>610m	>650m	
V	Faroe Plateau	1988-2016	>340m				>500m	
V	Faroe Bank	1988-2016	536m	560m	573m	593m	609m	640m

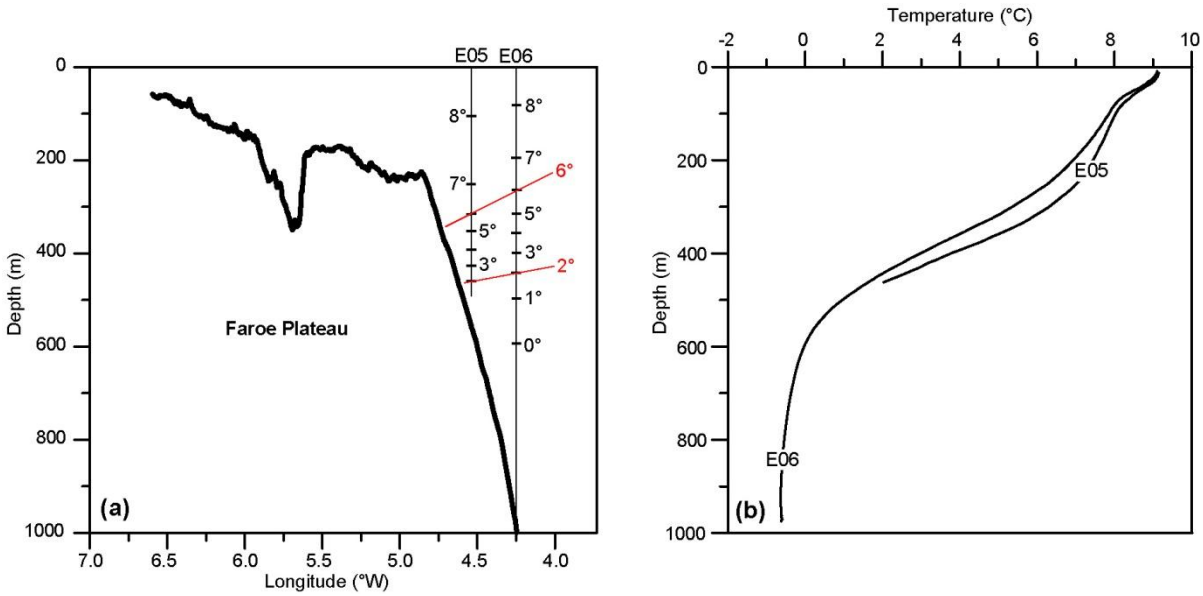

Figure 14. Temperature along section E. **(a)**: Average isotherm depths at standard CTD stations E05 and E06. Thin red lines show the depths of two selected isotherms extrapolated onto the bottom. **(b)**: Average temperature profiles at standard CTD stations E05 (94 occupations) and E06 (100 occupations).

A similar procedure may be used for the other standard sections except that we do not usually have similar long term deployment sites as well located on the other sections, but both section E (Figure 14) and section S (Figure 15) have standard stations so close to fairly steep slopes that extrapolation onto the bottom (thin red lines in the figures) seems reasonably accurate especially since these stations have been occupied quite frequently. On these two sections, we only have frequent CTD occupations on the Faroe side of the Faroe-Shetland Channel, but Table 3 includes some minimum isotherm depths on the Scottish slope bottom on section S based on 7 occupations of a standard station (S16, Figure 11) close to the Scottish slope.

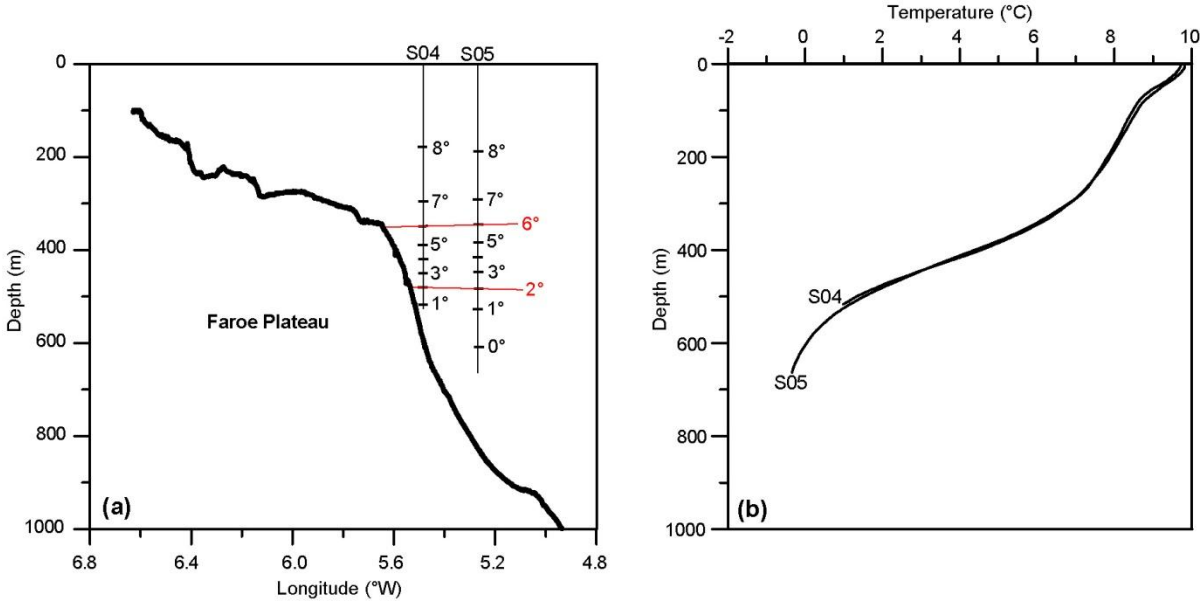

Figure 15. Temperature along section S. **(a)**: Average isotherm depths at standard CTD stations S04 and S05. Thin red lines show the depths of two selected isotherms extrapolated onto the bottom. **(b)**: Average temperature profiles at standard CTD stations S04 (80 occupations) and S05 (83 occupations).

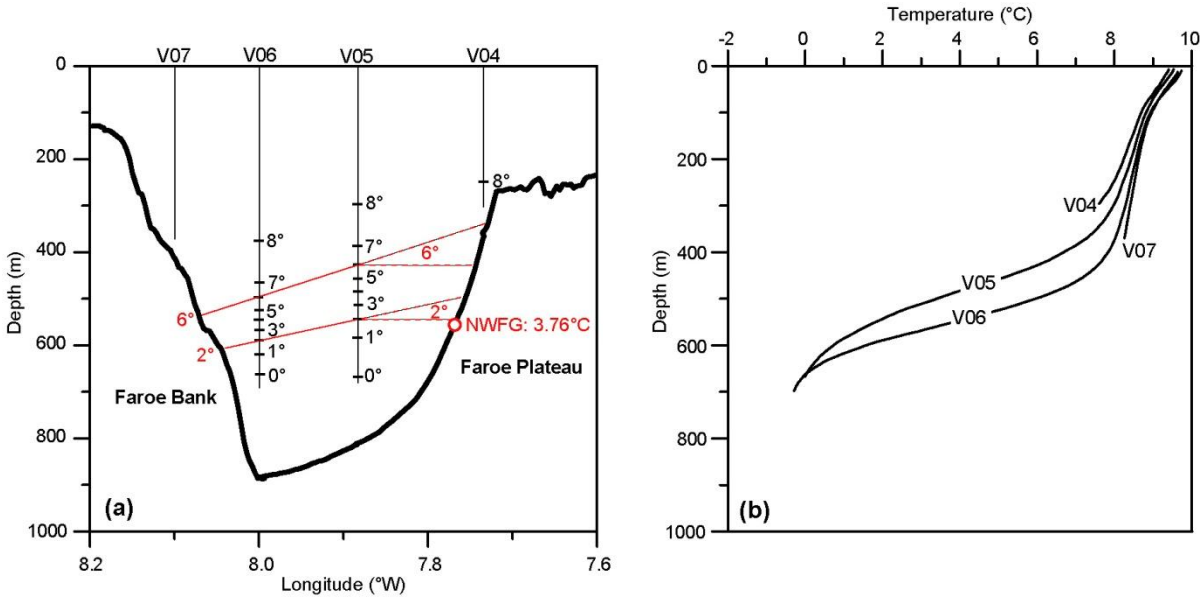

Figure 16. Temperature along section V. **(a)**: Average isotherm depths at standard CTD stations V04, V05, V06, and V07. Thin red lines show the depths of two selected isotherms extrapolated onto the bottom. The extrapolation towards the Faroe Plateau is fairly uncertain and two extreme versions are indicated by the hatched lines. Red circle labelled NWFG indicates the average bottom temperature from the ADCP deployment at NWFG (Table 1), located somewhat northwest of section V. **(b)**: Average temperature profiles at standard CTD stations V04 (120 occupations), V05 (133 occupations), V06 (131 occupations), and V07 (114 occupations).

For section V, extrapolation onto the bottom slope of the Faroe Plateau is more difficult due to the strong isotherm tilt, which is caused by the high vertical shear in the current. Most likely, this extrapolation is somewhere between the two alternatives indicated in Figure 16 by dashed lines for each of the isotherms 6°C and 2°C. In Table 3, only minimum depths are therefore indicated for where these two isotherms hit the Faroe Plateau slope. Figure 16 includes the average bottom temperature from deployment NWFG, which does not seem to be very consistent with the isotherms from the CTD stations, but note that this deployment was actually somewhat farther to the northwest from section V. On the Faroe Bank side of the channel, extrapolation seems much more straightforward and it is included in Table 3.

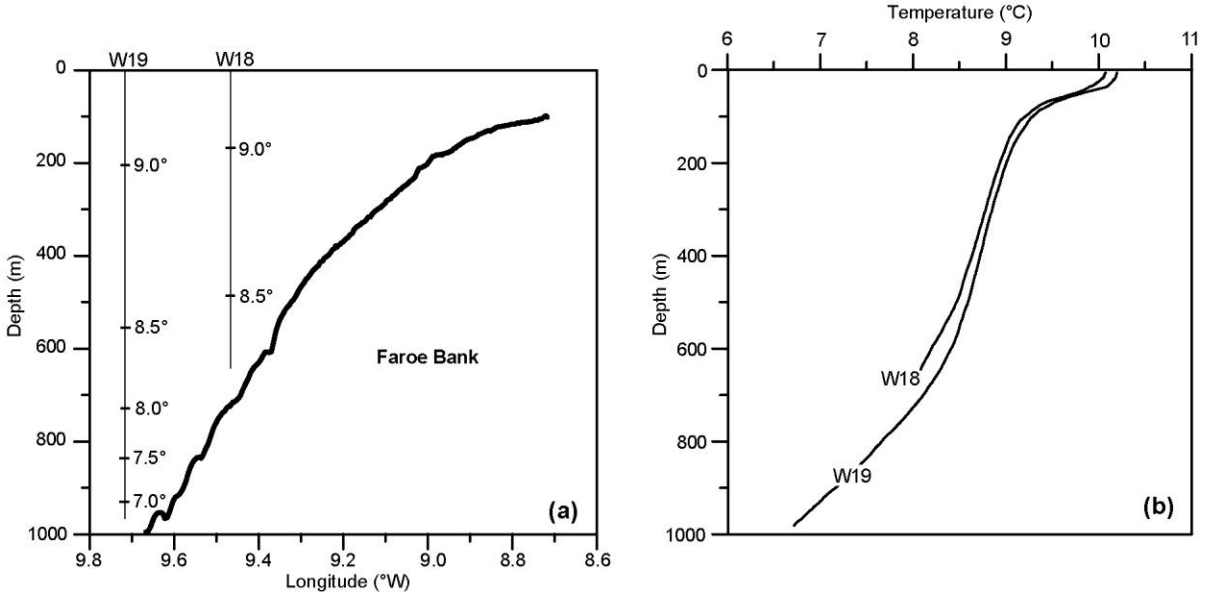

Figure 17. Temperature along section W. **(a)**: Average isotherm depths at standard CTD stations W18 and W19. **(b)**: Average temperature profiles at standard CTD stations W18 (54 occupations) and W19 (50 occupations).

The last standard section is section W (Figure 11), extending northwestwards from the Faroe Bank into the Iceland Basin (Figure 17). This section is not included in Table 3, but the figure indicates that the 6°C isotherm is below 1000 m depth on the slope north of Faroe Bank.

In addition to the average conditions, the CTD data from standard stations contains information about the temperature variability. This is utilized in Table 4 that lists temperature standard deviation at fixed levels down through the water column for ten standard stations. At shallow levels, the variability is dominated by seasonal and inter-annual variations of the Atlantic Water temperature. At deeper levels, we note especially the difference between section W and the other sections. Section W is affected only by Atlantic Water with small variations at the deep levels. On the other sections, the vertical movement of the boundary between Atlantic Water and Deep Water generates high variability at mid-levels. At larger depths on these sections, the standard deviations decrease to low levels as we descend into pure Deep Water with highly stable temperatures.

Table 4. Standard deviation of temperature (in °C) at fixed depths with 50 m interval at ten standard stations. N indicates number of occupations. For station W19, two extra depth levels are included.

St.	N	25m	75m	125m	175m	225m	275m	325m	375m	425m	475m	525m	575m	625m	825m	975m
N04	125	1.5	1.0	1.0	1.2	1.4	1.6	1.8	2.0	1.8						
N05	122	1.7	1.4	1.8	2.1	2.3	2.4	2.3	1.9	1.4	0.9	0.6	0.4	0.2		
E05	94	1.6	0.9	0.8	0.8	1.0	1.2	1.4	1.5	1.6						
E06	100	1.7	1.1	1.2	1.4	1.7	1.9	2.0	1.8	1.5	1.1	0.7	0.4	0.3		
S04	80	1.6	0.9	0.8	0.8	0.9	1.0	1.2	1.4	1.5	1.2					
S05	83	1.5	0.9	0.9	0.9	1.0	1.2	1.5	1.7	1.6	1.3	0.8	0.5	0.3		
V05	133	1.2	0.8	0.6	0.6	0.6	0.7	0.8	1.1	1.5	1.6	1.4	1.0	0.7		
V06	131	1.2	0.8	0.6	0.5	0.5	0.6	0.6	0.8	1.1	1.8	2.4	2.4	1.3		
W18	54	1.4	0.7	0.5	0.4	0.4	0.3	0.3	0.3	0.3	0.3	0.3	0.3	0.3		
W19	50	1.4	0.7	0.5	0.4	0.3	0.3	0.3	0.3	0.3	0.3	0.3	0.3	0.3	0.4	0.3

4 Bottom temperature from trawl-attached sensors

From 1999 to 2016, R/V Magnus Heinason took 4090 bottom trawl hauls, during which a temperature logger was attached to the trawl and thus measured bottom temperature. Temperature data from the loggers were stored every few minutes together with position of the ship, echo-sounder depth, trawl wire length, and some other parameters. During some of the hauls, the depth of the trawl was also recorded, but these data proved unreliable and have not been used. Altogether, the data set contained 91576 records of raw data from depths between 54 m and 688 m (Raw records, Table 5).

Table 5. Number of hauls and records in depth intervals as recorded by the echo-sounder onboard R/V Magnus Heinason. The number of "Raw" records indicates the original number, whereas the "Good" records are those that remained after quality control.

Depth interval (m):	0-99	100-199	200-299	300-399	400-499	500-599	600-699
No. Hauls:	402	2079	884	386	229	41	19
No. Raw records:	7719	48299	18710	8048	5307	1405	715
No. Good records:	6926	44122	16914	7355	4857	1297	689

Since the trawl is towed a considerable distance behind the ship, the position and depth as recorded by the ship do not represent the trawl or the bottom temperature accurately. For our purpose, the exact position is not critical, but the bottom depth is. Usually, the trawl is, however, kept at relatively constant depth during a haul. In only 5% of the hauls recorded did the bottom depth vary by more than 50 m during the haul. We, therefore, will use the position and bottom depth recorded by the ship to represent the measured bottom temperature.

The data were further quality controlled, checking for missing echo-sounder values and for suspicious spikes in the temperature and bottom values. This reduced the data set to a total of 82160 "Good" records (Table 5). As mentioned in the introduction, we will ignore the records from hauls shallower than 100 m, which leaves 75234 "good records" distributed over the Faroe Plateau and Faroe Bank (Figure 18).

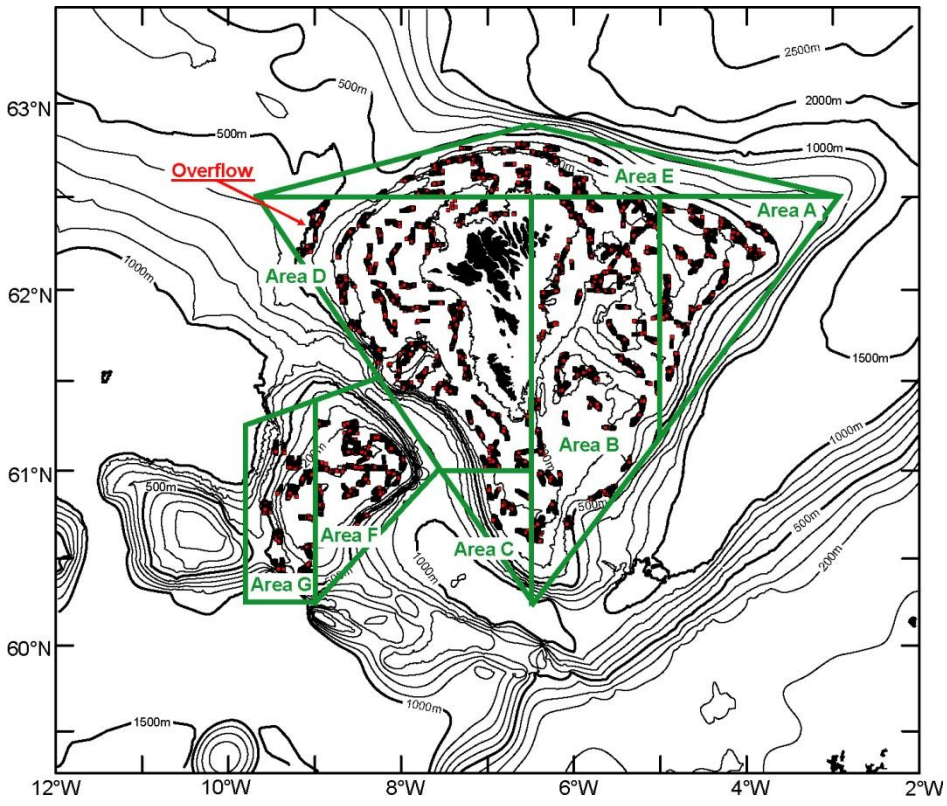

Figure 18. Locations of bottom temperature measurements with trawl-attached loggers outside the 100 m depth contour (red squares). The areas defined by thick green lines refer to Figure 19.

After some exploration of the data set, the region was divided into the seven areas shown in Figure 18 and the bottom temperature records from each area plotted against bottom depth (Figure 19). At a first glance, there is a

surprising bimodality in the shallowest records for all the areas that have records that are shallower than ≈150 m. Closer inspection reveals, however, that this is due to seasonal variation. The warm records (>9°C) were all acquired in August, September, or October, whereas most of the cold records (<9°C) were acquired in February, March, or April (Figure 20). The lack of intermediate (≈9°C) bottom temperature records shallower than 150 m is, no doubt, due to the lack of trawl hauls in the intermediate months.

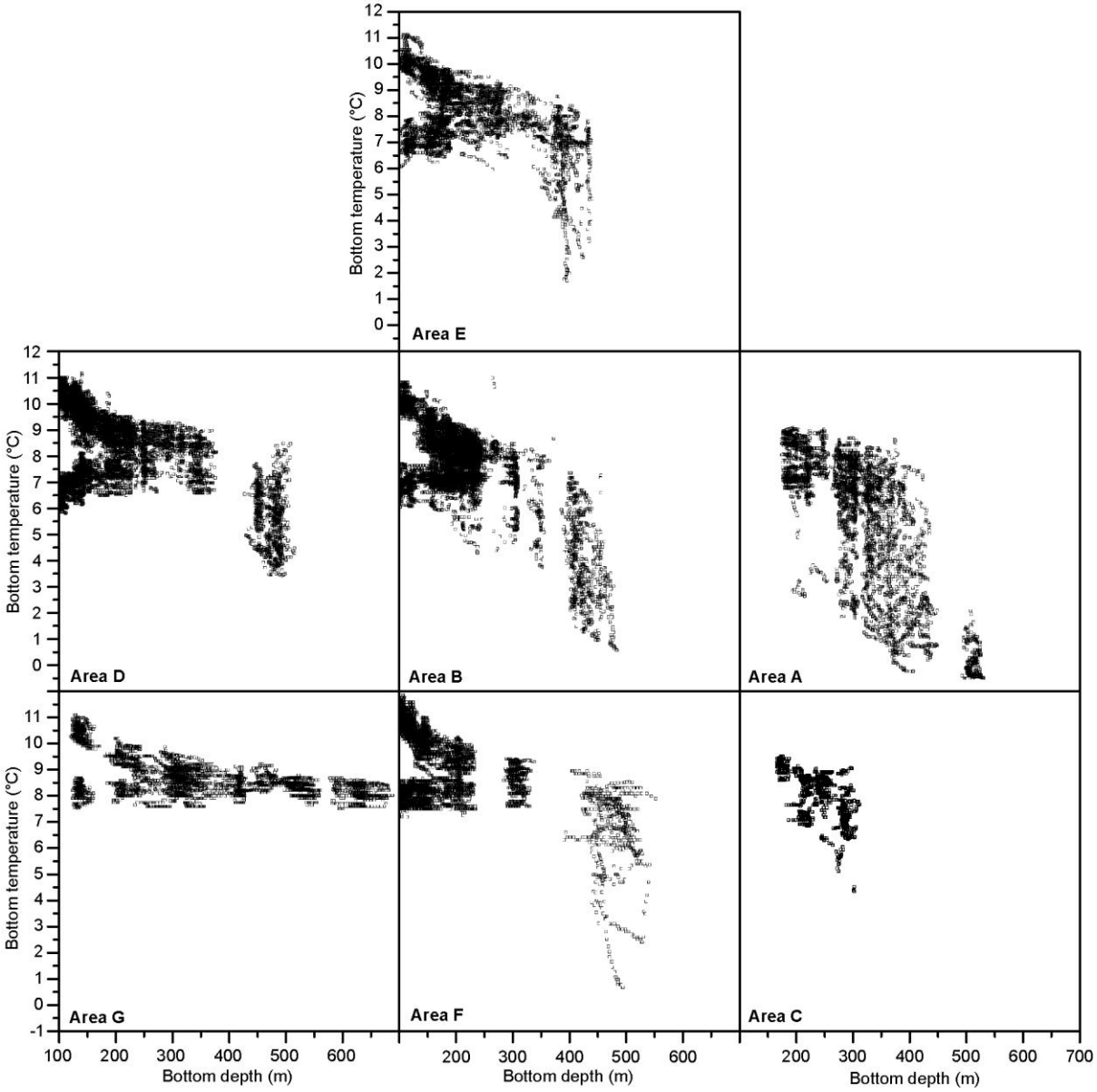

Figure 19. Bottom temperature plotted against bottom depth from trawl-attached temperature loggers distributed in the areas shown in Figure 18.

Closer inspection of Figure 19 reveals considerable differences between the different areas. Most pronounced is the difference between area G and all the others in that the water in area G remains warmer than 7°C even deeper than 600 m, whereas all the other areas include records with much lower bottom temperatures. Although less pronounced, there are, however, also differences between areas A to F. To get a more quantitative impression of this, the bottom temperature records were split into 50m depth intervals and averages and standard deviations calculated for each interval (Table 6).

Table 6 is in reality three separate tables with the top one listing the number of records in each depth interval for each area and we see that most of the areas have only few records at greater depth. To reduce biases from this, averages (middle table) and standard deviations (bottom table) have only been calculated for depth intervals with at least 20

records. This does not, however, guarantee that the calculated values are representative since all the records may be from just one or only a few hauls.

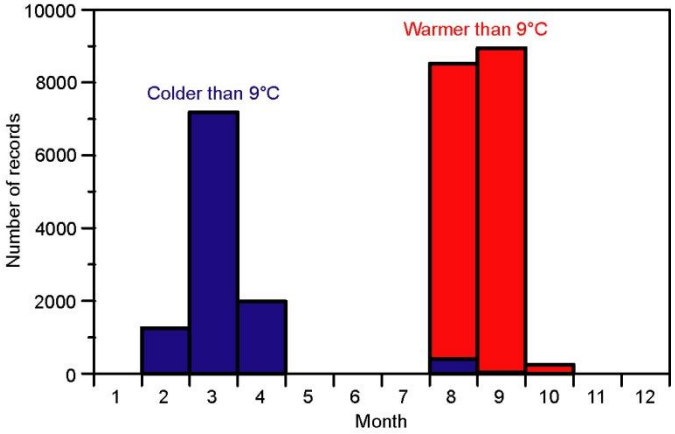

Figure 20. Monthly distribution of bottom temperature records between 100 m and 150 m depth that were colder than (blue bars) or warmer than (red bars) 9°C, respectively.

The average bottom temperatures in Table 6 confirm the special conditions in the deep parts of area G, but also indicate some other features. Firstly, we note that areas F and G are warmer than all the others at all depths. Secondly, the western and northern regions in areas D and E seem to be generally warmer than the eastern and southern regions in areas A, B, and C. But, perhaps most remarkable, area A is colder than all the others at all depths, which indicates that cold waters from the north ascend and flow over the eastern tongue of the Faroe Plateau.

Another remarkable feature is the occurrence of water colder than 4°C in the northwestern corner of area D indicated by the red arrow in Figure 18. This is a clear indication that this area, which ranged between 450 and 500 m in bottom depth, is affected by Deep Water either from FBC-overflow or IFR-overflow.

Table 6. Number of records (top table), average bottom temperature (°C, middle table), and standard deviation of bottom temperature (°C, bottom table) for all seven areas in Figure 18 distributed into 50m-intervals with the centre depth shown in the top line of each table. Averages and standard deviations are only listed if the number of records was more than 20.

	125m	175m	225m	275m	325m	375m	425m	475m	525m	575m	625m	675m
A	0	660	1040	1297	1535	1022	404	10	389	0	0	0
B	3214	6053	4788	391	600	101	735	175	0	0	0	0
C	0	212	596	475	26	0	0	0	0	0	0	0
D	10318	3590	1961	1170	770	237	172	1239	39	0	0	0
E	1658	2625	852	945	214	693	329	0	0	0	0	0
F	11126	2106	1791	246	669	3	184	442	144	1	0	0
G	2252	308	898	464	1223	262	819	348	607	117	527	162

	125m	175m	225m	275m	325m	375m	425m	475m	525m	575m	625m	675m
A		7.9	7.6	6.7	5.8	4.2	2.7		0.1			
B	8.9	8.1	7.8	7.8	6.8	6.0	4.2	2.9				
C		9.0	8.1	7.6	7.0							
D	8.9	8.7	8.4	8.3	8.1	7.7	6.1	5.7	5.8			
E	8.9	8.5	8.4	8.2	7.9	6.6	6.6					
F	9.8	9.1	9.0	8.7	8.7		7.5	6.8	6.3			
G	9.6	9.3	9.0	8.7	8.6	8.5	8.4	8.6	8.3	8.2	8.1	8.1

	125m	175m	225m	275m	325m	375m	425m	475m	525m	575m	625m	675m
A		0.8	1.0	1.6	1.9	2.4	1.7		0.5			
B	1.5	0.8	0.7	0.8	1.0	1.4	1.6	1.4				
C		0.4	0.7	0.9	0.9							
D	1.5	1.0	0.7	0.6	0.7	0.7	0.9	1.1	1.4			
E	1.4	1.0	0.7	0.6	0.5	1.4	1.2					
F	1.4	0.9	0.7	0.6	0.5		1.2	1.7	1.6			
G	1.2	1.0	0.6	0.6	0.4	0.5	0.3	0.2	0.3	0.3	0.3	0.2

5 Bottom temperature from Seagliders

From 2006 to 2009, the University of Washington, Seattle, ran a campaign with Seagliders travelling back and forth between Faroes and Iceland, focusing on the Atlantic (western) side of the Iceland-Faroe Ridge (Beaird, Rhines, and Eriksen, 2013). In order to map the overflow, the Seagliders went close to bottom and hence measured bottom temperature. These observations were kindly made available by Nick Beaird. The data set contains 5616 records with position, date, bottom depth, and bottom temperature. The Seagliders usually did not dive deeper than 1000m and most of the data are from bottom depths between 400m and 900m (Figure 21).

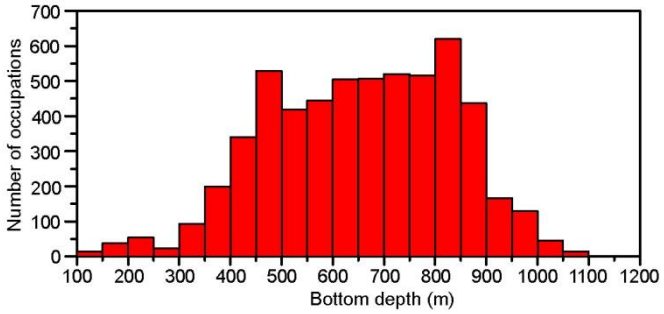

Figure 21. Histogram of bottom depths observed by the Seagliders.

In the following treatment, the data are first split into two regions by the 62°N latitude. In the northern of these two regions, most of the observations are from the Atlantic flank of the Iceland-Faroe Ridge (IFR), over which, water colder than 2.5°C (blue dots in Figure 22) is seen to extend from the exit of the Faroe Bank Channel (FBC) northwestwards to the "corner" around 63°N. Most of the flank is, however, dominated by water of more intermediate temperature (green dots in Figure 22).

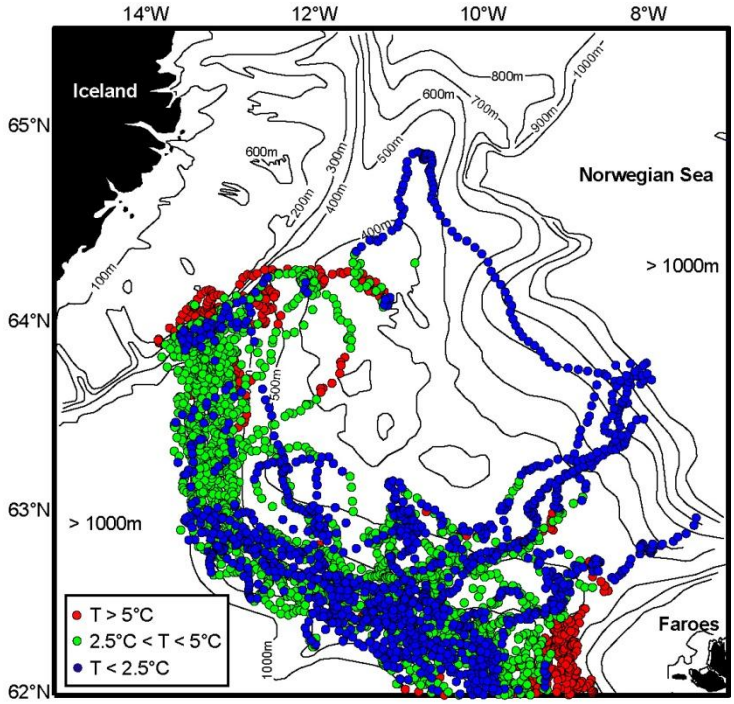

Figure 22. Bottom temperatures observed by Seagliders north of 62°N divided into three temperature classes.

The region north of 62°N is further subdivided into four sub-regions (Figure 23). In each of these sub-regions, the isobaths are approximately parallel except for sub-region G-2, where they are close to being circles around point G (63°N, 12°W). In the top panels of Figure 24, the bottom depth is plotted against a parameter that is roughly perpendicular to the isobaths in each sub-region as indicated by the cyan arrows in Figure 23. For G-1 and G-4, this parameter is longitude. For G-2, it is the radial distance from the point G shown in Figure 23. For G-3, it is the latitudinal displacement of each point from the top boundary of sub-region G-3.

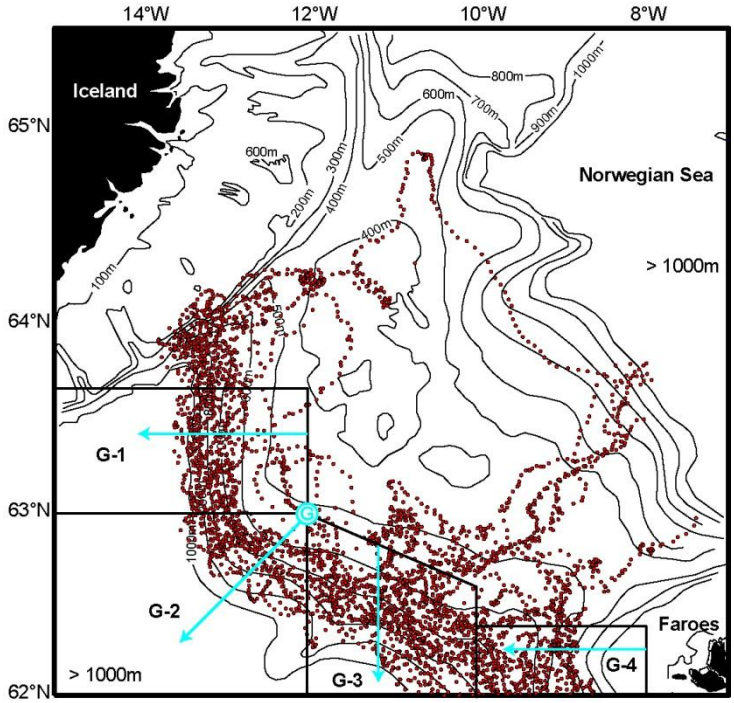

Figure 23. Positions of bottom temperature measurements north of 62°N by Seagliders from Nov 2006 to Nov 2009. The four sub-regions in Figure 24 are shown and the cyan arrows indicate the x-axis in that figure for each sub-direction.

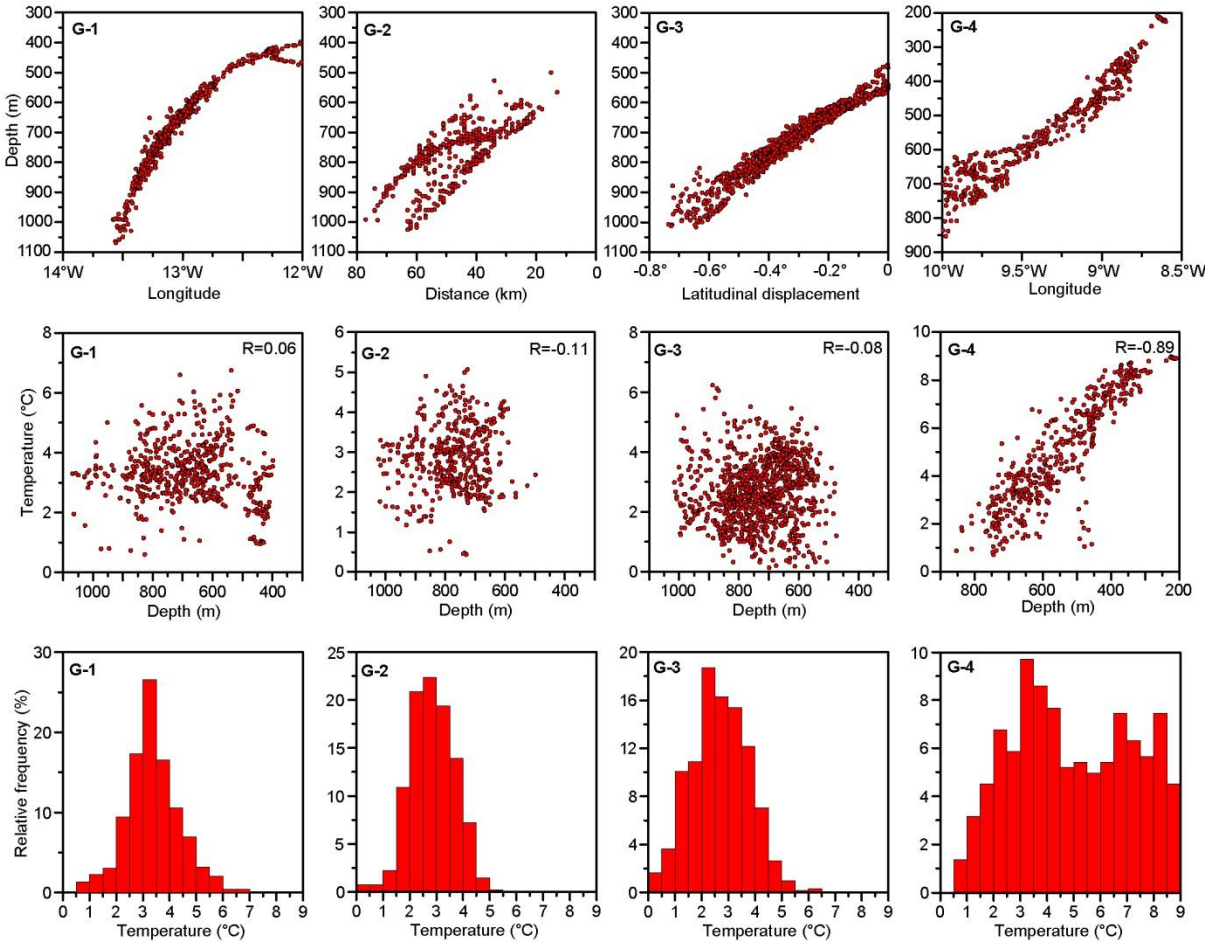

Figure 24. Characteristics of the four sub-regions in Figure 23. **Top panels:** Bottom depth plotted against longitude (G-1 and G-4), radial distance from point G (G-2), or latitudinal displacement from top boundary of the sub-region (G-3). **Middle panels:** Bottom temperature plotted against bottom depth with the correlation coefficient between the two indicated. **Bottom panels:** Histograms of bottom temperature.

If the isobaths were perfect concentric circles in sub-region G-2 and parallel lines in the other sub-regions, then the points in the top panels of Figure 24 should fall on a single curve for each sub-region. In G-1 and G-3 they do that to a high degree and reasonably well in G-4, as well. This indicates that most of the records have been acquired close to the bottom so that the temperature values will represent bottom temperature fairly well. The discrepancies are easily explained by the deviations of bottom topography from the idealized circular and linear picture, although there may also be a few records that do not really reflect bottom conditions.

This indicates that the high variability in the middle panels of Figure 24 is real and not due to records being sampled too far away from the bottom. For sub-regions G-1, G-2, and G-3, the middle panels show no systematic variation of bottom temperature with bottom depth and the histograms for these sub-regions in the bottom panels should therefore represent the whole sub-region between 500m and 1000m fairly well. Consistent with Figure 22, the coldest component (T < 2.5°C) dwindles on the way from G-3, through G-2 to G-1. Apart from that, the histograms from these three sub-regions look fairly similar (bottom panels in Figure 24).

In sub-region G-4, there is a much clearer decrease in bottom temperature with depth as also indicated by the correlation coefficient (R = -0.89). A deviation from this is shown by a few very cold records at depths between 400m and 500m. This is in the same regions as the observations of relatively low temperatures in trawl-attached loggers (Figures 18 and 19, area D) and the coldest of these observations are shown as six blue circles close to the 450m isobaths in Figure 25.

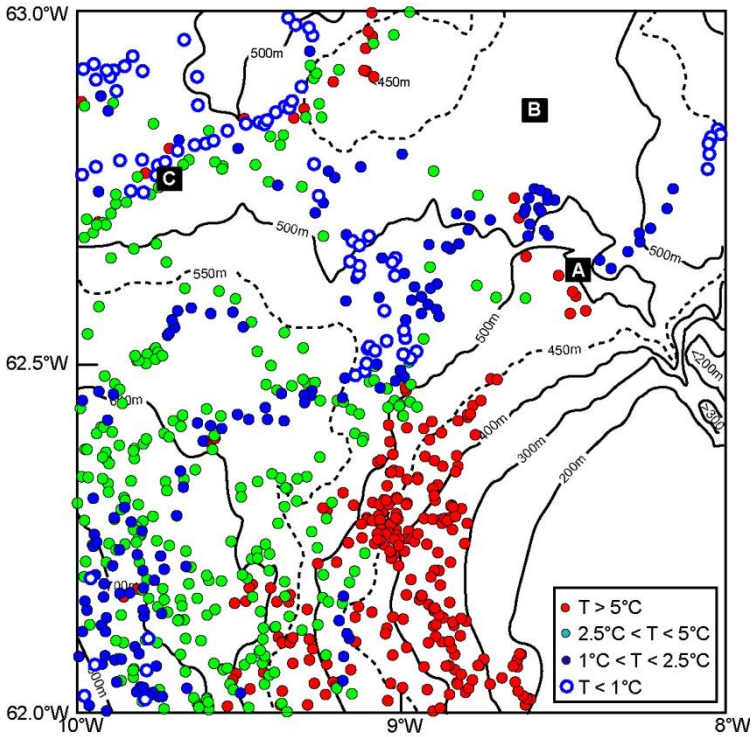

Figure 25. Bottom temperatures from Seagliders in the region connecting the Faroe Plateau to the Iceland-Faroe Ridge divided into four temperature classes. Black squares labelled A, B, and C mark the locations of ADCP moorings IFRA, IFRB, and IFRC, respectively (Table 1). The bottom topography is from ETOPO1.

The most likely origin of these cold bottom waters would seem to be FBC-overflow, but they are at shallower depths than might have been expected (see also Figure 26). Another possibility is overflow across the southeasternmost part of the Iceland-Faroe Ridge. That there is IFR-overflow in this region seems quite clear from Figure 25, which shows very cold (< 1°C) bottom water around (62.5°N, 9°W) in the channel descending from the deepest passage across the ridge. From the temperatures at site IFRA (Table 1), cold water enters this channel frequently and would be expected to descend through the channel. Alternative pathways crossing the ridge at more westerly locations might also be indicated by Figure 25.

In the region south of 62°N, the bottom temperatures measured by the Seagliders are dominated by the effects of the FBC-overflow flowing into the Iceland Basin (Figure 26). The intensive mixing downstream of the secondary FBC sill warms the bottom water, but water colder than 2.5°C (blue circles in Figure 26) dominates the Faroe side of the channel between 700m and 1000m depth. There is, however, considerable temporal variation (Geyer et al., 2006) as indicated by the occurrence of warmer water (green circles) in this region.

On the Faroe Bank side of the FBC, the cold FBC-overflow water stays fairly deep and there is a sharp boundary towards warmer water so that the bottom temperatures seldom are in the intermediate range (2.5°C to 5°C). West of the Faroe Bank, warm water extends all the way down to 1000m and deeper (red circles in Figure 26).

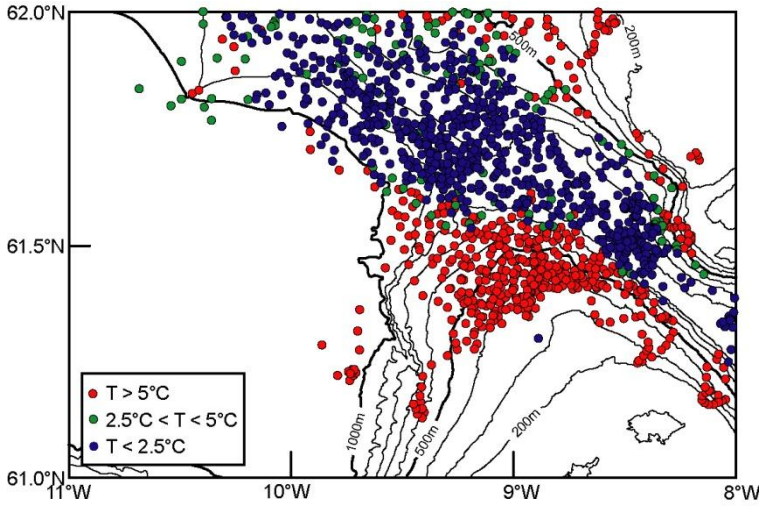

Figure 26. Bottom temperatures observed by Seagliders south of 62°N divided into three temperature classes.

6 Synthesis of bottom temperature measurements

Having gone through the various data sets that contain information on bottom temperature, this section aims at synthesizing this information into a consistent picture. As noted in the introduction, we focus on the areas most relevant for Faroese fisheries, for which there is adequate data coverage. This is primarily the Faroe Plateau and Faroe Bank regions. We will largely ignore areas deeper than 1000 m and for the highly variable regions on the Iceland-Faroe Ridge, the available evidence is too sparse to allow a detailed picture to be drawn. To structure the presentation, we split the region into three separate domains as illustrated in Figure 27, but it should be emphasized that the domains are not very exactly defined and their borders cannot be accurately drawn.

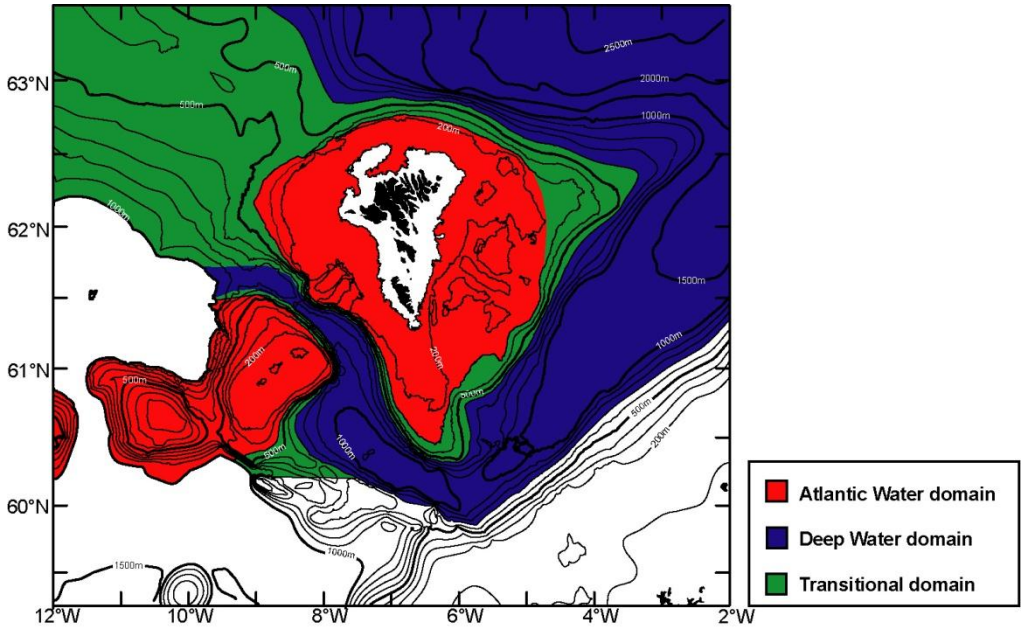

Figure 27. Approximate geographical extents of the three domains. White areas are not discussed.

6.1 The Atlantic Water domain

All the shallow regions on both the Faroe Plateau and on the Faroe Bank are dominated by the warm Atlantic Water. From Table 1, we see that the four shallowest sites with depths down to 300 m were warmer than 7°C on average with temperature standard deviations less than 1°C. This does not imply that cold water cannot reach areas shallower than 300 m as exemplified by the minimum temperatures listed in Table 1, but these occurrences are not frequent and water colder than 5°C is seldom experienced in most areas shallower than 300 m (Figure 28).

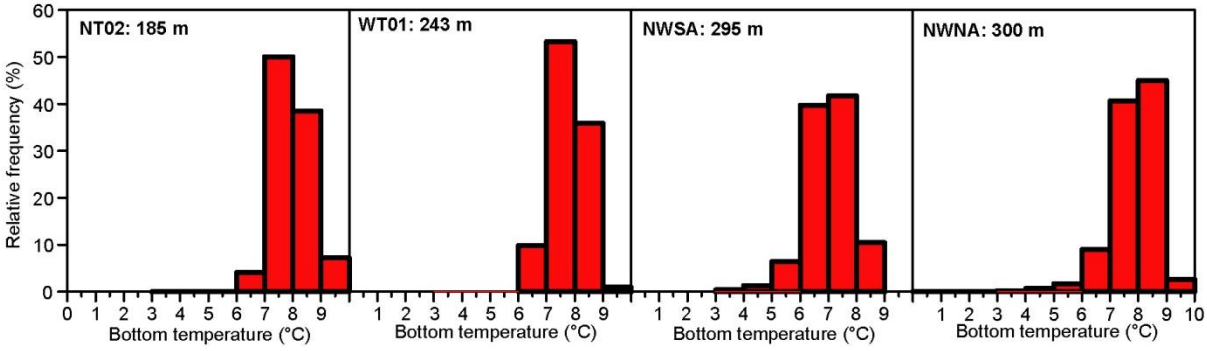

Figure 28. Frequency distributions (histograms) of measured bottom temperatures at four mooring sites listed in Table 1.

On the Faroe Plateau, the Atlantic Water domain may therefore in most areas be defined as the area shallower than 300 m, although with two exceptions. Firstly, the shallowest parts of the shelf are strongly affected by winter cooling from the atmosphere and behave differently from the deeper parts of the shelf area. As mentioned previously, this has been

thoroughly discussed elsewhere (e.g., Larsen et al., 2008, 2009) and is not repeated here. In Figure 27, we have indicated that by making the area within the 100 m isobaths white.

Secondly, the eastern parts of the Atlantic domain on the Faroe Plateau are somewhat colder than the western parts. This is perhaps most clearly seen in Figure 19 and in Table 6 and is most pronounced in the easternmost tongue of the Faroe Plateau – area A on Figure 18. For this area, Table 6 shows much more temperature decrease with depth (both from 225m to 275m and from 275m to 325m) than the other areas. Also, the standard deviations in Table 6 for all the depth intervals from 225m to 375m are considerably higher in this area than elsewhere. In Figure 27, the Atlantic domain therefore does not extend all the way to the 300 m isobath in this area.

In the northwestern corner of the Faroe Plateau – between the sill region of the Faroe Bank Channel and the bridge to the Iceland-Faroe Ridge – the Deep Water from the FBC-overflow has descended and the Atlantic Domain seems to extend somewhat deeper, at least to 400m depth according to the bottom trawl loggings (Figure 19, area D) and the Seaglider observations (Figure 25 and Figure 26).

On the western banks - Faroe Bank and Bill Bailey's Bank – the Atlantic domain extends to larger depths than on the Faroe Plateau. Towards the Faroe Bank Channel, Figure 16 and Table 4 indicate that it extends to at least 400 m depth in the region south of the sill. As we progress northwards, the FBC-overflow exits the narrow channel and the deep boundary of the Atlantic domain deepens (Figure 26). On standard section W (Figure 11), the Atlantic domain can be said to extend to at least 1000 m depth since the water at this depth will normally be warmer than 6°C (Figure 17 and Table 4). This picture – with the Atlantic layer extending to at least 1000 m – seems to apply also to the western slope region of the Faroe Bank (area G in Figure 19) as well as the banks farther west (Figure 3), but on the southern side of Faroe Bank, overflow across the Wyville Thomson Ridge limits the depth of the Atlantic domain.

The Atlantic domain, thus, has different vertical extent in different areas and it is not horizontally homogeneous, either. Rather, the Atlantic water loses heat to the atmosphere and cools on its way from the west to the east (Figure 2a). From Table 6, this cooling generates a temperature difference of slightly more than 1°C from the western banks to the eastern areas on the Faroe Plateau. In spite of this, the temporal variation seems to be very similar in different areas (Larsen et al., 2012) and we can use the temperature of the high-salinity core in the Faroe Bank Channel as an indicator of both long-term variations (Figure 29a) and seasonal variation (Figure 29b). Since these two types of variation are mixed into the observed time series, we use an iterative procedure to disentangle them as described in Appendix B.

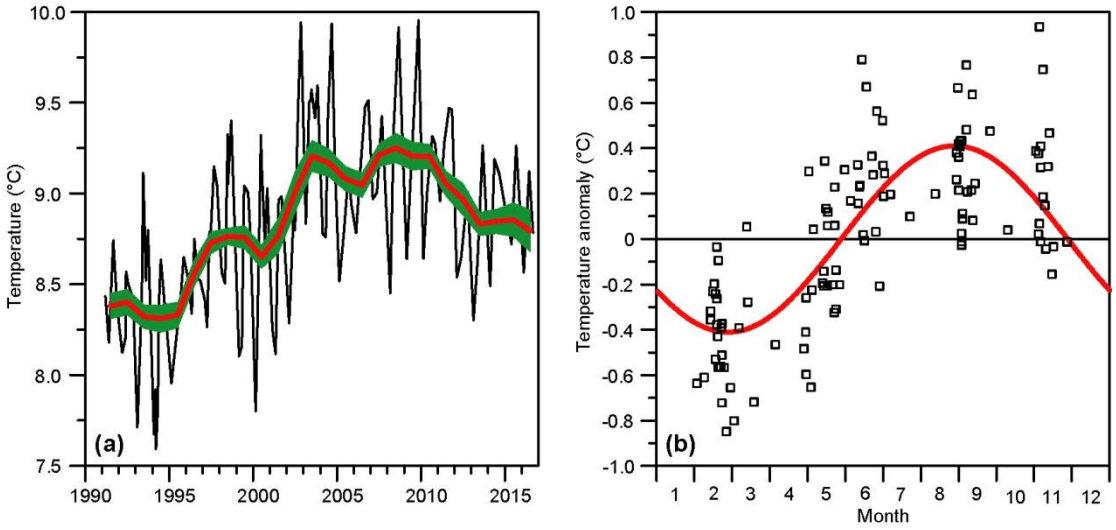

Figure 29. Temperature of the high-salinity core in the Faroe Bank Channel based on 114 CTD cruises in the period 1991 – 2016. **(a):** Individual values from each cruise (black line) and 3-year running mean of de-seasoned temperature (thick red line with green area indicating ± 1 standard error). **(b):** Squares indicate temperature anomaly of individual value from 3-year running mean for same year. Red line indicates the sinusoidal seasonal fit.

The long-term variation of the Atlantic Water temperature (Figure 29a) shows a warming of almost 1°C from 1994 to 2003. Thereafter, the temperature remained fairly stable until 2010, after which it has decreased by almost 0.5°C. The seasonal variation of the high-salinity core in the Faroe Bank Channel (Figure 29b) fits fairly well to a sinusoidal variation with a correlation coefficient of R = 0.76. The fit gave a seasonal amplitude of 0.41°C with maximum temperature on day number 240 (ultimo August).

This value for the seasonal amplitude is probably representative for the core of Atlantic water reaching Faroese waters, but for shallow areas, we should expect considerably larger amplitudes. This is also the impression that one gets from Figure 19 and it is elaborated in Figure 30. In this figure, the bottom temperature measurements from trawl-attached loggers were divided into 50m depth intervals for the Faroe Plateau and for Faroe Bank separately and separate histograms made for hauls in winter (blue bars) and summer (red bars). To correct for the confounding effects of long-term variations, the 3-year running mean temperature in the core of Atlantic Water in the Faroe Bank Channel (Figure 29a) was subtracted from the measured temperature and the histograms show the resulting anomaly.

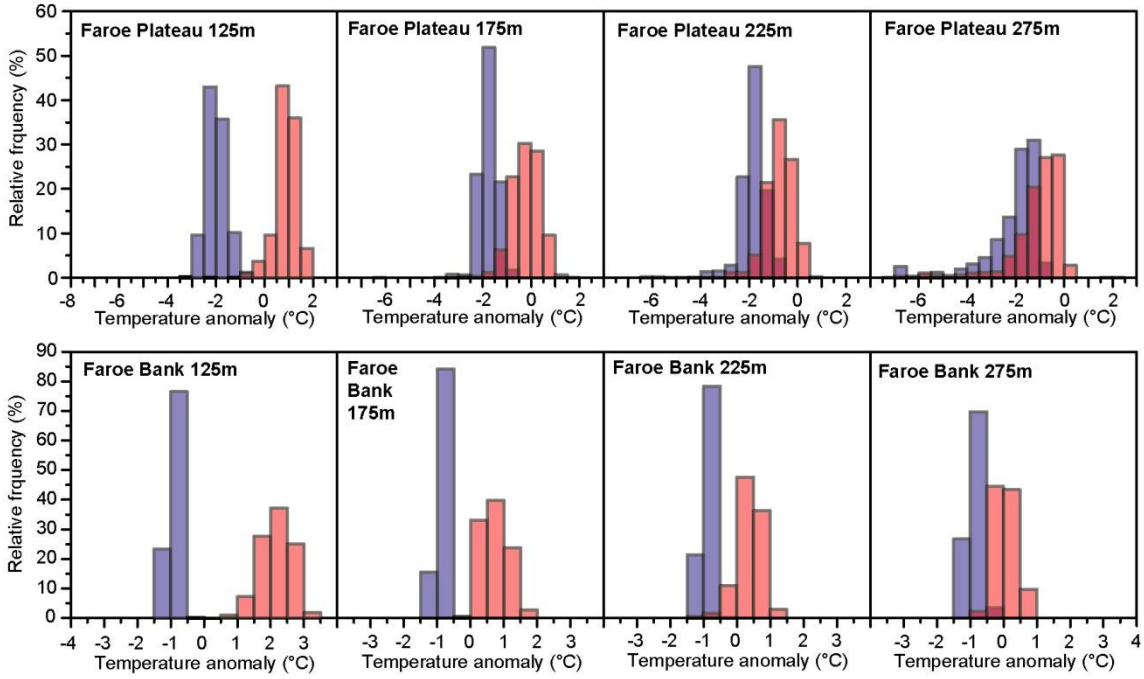

Figure 30. Seasonal bottom temperature variation for different depth intervals on the Faroe Plateau (upper panels) and on the Faroe Bank (lower panels) based on measurements from trawl-attached loggers. Each panel shows the relative frequency (histogram) of the temperature anomaly (measured temperature minus 3-year running mean) for one 50m depth interval labelled by the centre depth. Blue bars are for months February to April. Red bars are for months August to October. The bars are semitransparent to show overlaps.

Both the Faroe Plateau and Faroe Bank show the same tendency of decreasing summer-winter difference with depth. At 125m depth (depth interval from 100m to 150m), the difference between the red and the blue bars in Figure 30 is ≈3°C. This difference is reduced to ≈1°C at depth 275m (depth interval 250m to 300m), which is of similar magnitude as the seasonal range of the incoming Atlantic Water as represented by Figure 29b and also similar to the seasonal range at ADCP site NWNA at 300m depth (Figure 6). The enhanced seasonal range is also evident at 175m depth and perhaps even at 225m depth.

6.2 The Deep Water domain

In the scientific literature, the term “Deep Water” has been used to denote many different water masses with different origins and definitions. Here, we use it to denote the cold and relatively homogeneous water found at depth around much of the Faroe Plateau. From the average temperature profiles in Figure 13 to Figure 16, the temperature starts to become homogeneous at around 600m depth where it typically falls below 0°C. In Figure 27, we have therefore used the 600m isobath on the Faroe Plateau for its upper boundary in most directions. On the eastern Faroe Bank slope and the Scottish side of the Faroe-Shetland Channel, the boundary is deeper (Table 3) and there we have used the 700m isobath.

The Deep Water crosses the submarine ridge system between Iceland and Scotland in three regions (Figure 2b). The IFR-overflow and the WTR-overflow are weak and intermittent. In Figure 27, the regions affected by these two overflows are therefore in the Transitional domain. The FBC-overflow, in contrast, is very persistent and the sill of the Faroe Bank Channel is continuously covered by cold water as documented by the low maximum temperature for site NWFB in Table 1. Downstream from the sill, areas with undiluted Deep Water may also be found, but the encounter between the Deep

water and the Atlantic Water initiates strong mixing that involves highly variable – and in some locations even periodic (Geyer et al., 2006) – distributions of water masses and bottom temperature.

6.3 The Transitional domain

The Transitional domain may be divided into three sub-domains: the Faroe Plateau, the Iceland-Faroe Ridge, and the Faroe Bank.

6.3.1 The Transitional domain on the Faroe Plateau

Although the boundaries of the Transitional domain on the Faroe Plateau cannot be localized or even defined very accurately, it is generally at bottom depths between 300m and 600m that we find the highest bottom temperature variability in most regions on the Faroe Plateau. The most comprehensive data set on bottom temperature in this domain is from the mooring sites (Figure 31) where regular bottom temperature measurements have been acquired at least every hour (typically every 20 minutes) over several months (Table 1 and Table A1).

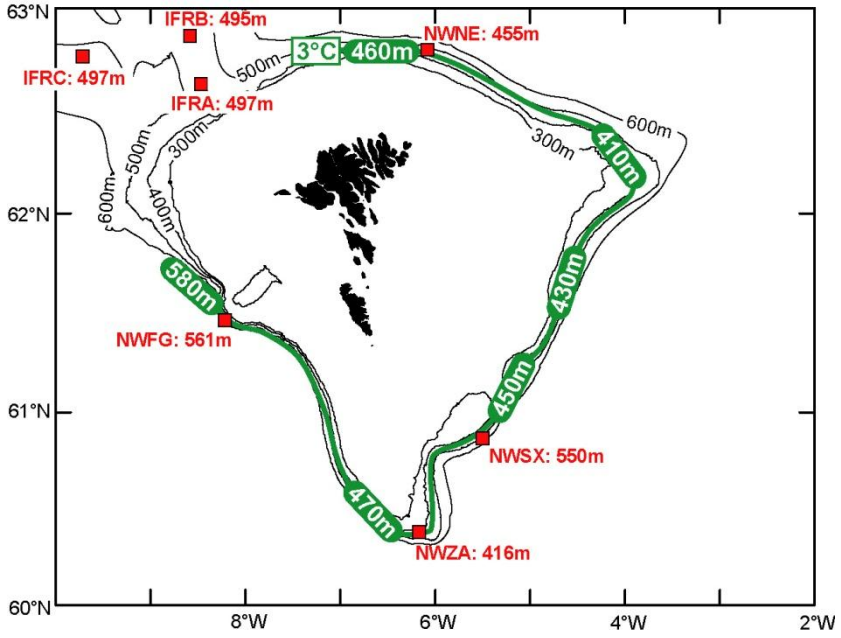

Figure 31. Mooring sites in the transitional domain (red squares) and average depth of the 3°C isotherm around the Faroe Plateau (thick green line with depth indicated at locations with good data coverage).

The longest time series is from mooring site NWNE, which is at depth 455m, halfway between the 300m and the 600m isobaths. This site has been occupied for a total of 3852 days in the period 2000-2015 (Table 1) and, thus, ought to give a reliable picture of the bottom temperature and its variations at this location. From the average temperature (3.15°C) at NWNE, this site should be located close to the 3°C isotherm associated with the average bottom temperature field. This isotherm may be used as an indicator for the centre depth of the Transitional domain and our best estimate of its depth around the Faroe Plateau is plotted in Figure 31, based on the evidence presented earlier in the report.

The depth values for the 3°C isotherm, shown in Figure 31, are of course associated with some uncertainty. At NWNE, this uncertainty is small. At the other locations, the values are more uncertain and should not be interpreted too strictly. They do reflect, however, two features, clearly supported by the data. Firstly, the 3°C isotherm and Transitional domain as a whole seem to be lifted on the order of 50m as the water flows over the eastern tongue of the Plateau (Figure 19 and Table 6).

Secondly, the isotherms descend from the southern tip of the Plateau – around NWZA – to the sill of the Faroe Bank Channel close to NWFG. This is supported by the high average bottom temperature at NWFG (Table 1), but it is also to be expected from basic physical arguments. As the overflow water approaches the narrow sill region, it accelerates, which requires a conversion of potential to kinetic energy that is acquired by a deepening of the isopycnals and hence also isotherms. A rough estimate of this deepening, ΔD, may be obtained by using the Bernoulli equation for a two layer system with initial speed zero and sill speed U:

$$\Delta D = \frac{\rho \cdot U^2}{2 \cdot g \cdot \Delta\rho} \qquad (1)$$

With U = 1 m s^{-1} and the density difference between layers $\Delta\rho$ = 0.5 kg m^{-3}, this equation yields: ΔD ≈ 100m, which is quite consistent with the observed values. We do not have much observational evidence for where along the route from NWZA to NWFG this deepening occurs but, from the argument above, it should be close to the sill where most of the increase in U^2 occurs. This is also the conclusion from Figure 16, which indicates considerable isotherm deepening along the short distance from section V, upstream of the sill, to site NWFG, located at the sill.

Combining the long-term measurements at mooring sites NWNE and NWNA with CTD data from standard sections, depths of the average isotherms for the temperature range 6°C to 1°C on section N were listed in Table 3. We find that the average bottom temperature typically decreases by 1°C for every ≈30m depth increase. This applies to the temperature range from 6°C to 2°C, whereas the 2°C isotherm and the 1°C isotherm were separated by ≈40m in bottom depth. For other locations on the Plateau, the data coverage is less comprehensive but, generally, the same pattern seems to apply (Table 3).

In the Transitional domain, the instantaneous temperature is, however, most of the time considerably different from the average temperature as seen in the top panels in Figure 32. At site NWNE, the instantaneous temperature was more than ±1°C different from (higher or lower than) the average temperature 64% of the time, and 34% of the time, the difference was more than ±2°C. At the other sites in Figure 32, the variability was not quite as high, especially at NWSX, which was close to the lower boundary of the Transitional domain.

Some of this variability – especially in the shallower part of the Transitional domain - may derive from long-term (Figure 29a) or seasonal (Figure 29b) variations of the Atlantic Water temperature. As noted previously (Figure 5 and Figure 6), these signals are difficult to identify in the observations, possibly because they are masked by the high short-term variability. The short-term variability is illustrated in the lower panels in Figure 32, which show histograms of the temperature changes from one day to the next for the four mooring sites in the Transitional domain on the Faroe Plateau. At site NWNE, the bottom temperature changed by more than ±1°C between days 28% of the time. At the other sites, changes of this magnitude were less frequent but still occurred 19% of the time at both NWZA and NWFG.

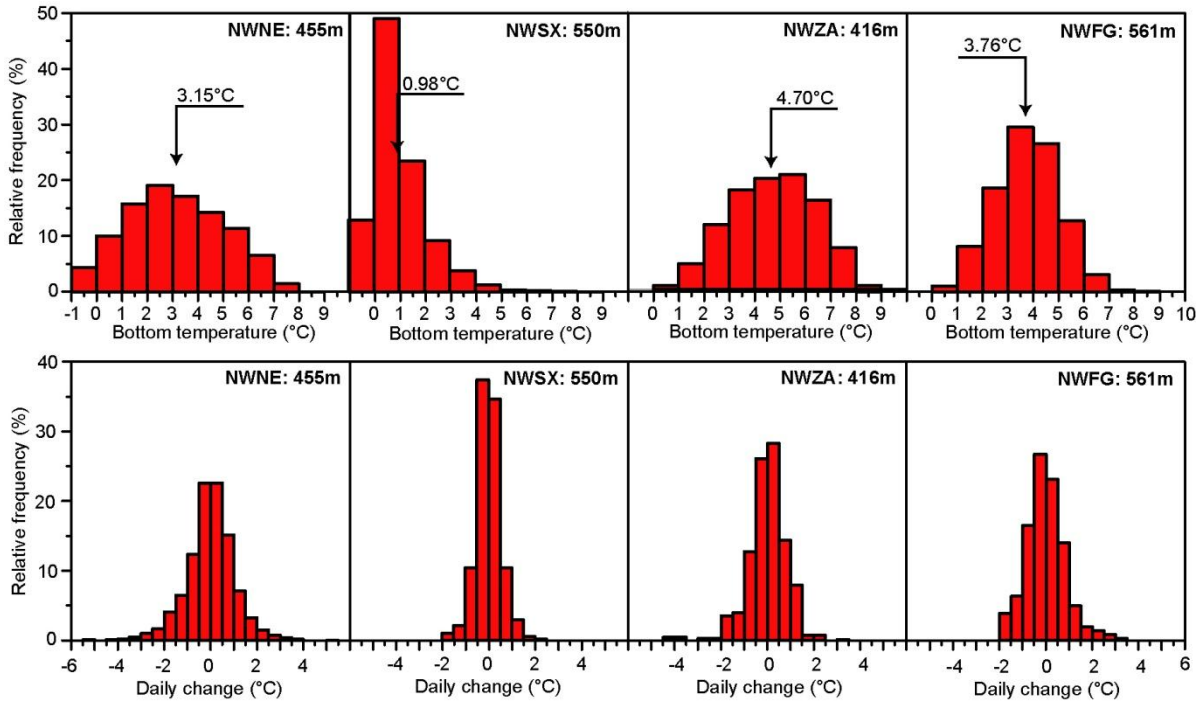

Figure 32. Bottom temperature variability at mooring sites in the Transitional domain on the Faroe Plateau. Top panels show relative frequency (histogram) of bottom temperature at each site with the average temperature indicated by the arrow. Bottom panels show relative frequency (histogram) of the daily averaged temperature change from one day to the next.

Since the lower panels in Figure 32 show changes in daily averaged temperatures between two consecutive days, they underestimate the short-term variability to some extent, as there are also variations on hourly or even shorter time scales. In Table 2, these variations were quantified by the root-mean-square value $<T_i'>$ of the difference between instantaneous and daily averaged temperature. At sites NWNE, NWZA, and at NWFG this value was ≈0.8°C whereas it was ≈0.5°C for site NWSX. At all four of these sites, the correlation coefficient between tidal temperature anomaly and tidal speed was highly significant (Table 2) and all the sites also exhibited a consistent tidal current direction associated with the time of maximum temperature each day (Figure 7).

For the sites NWNE, NWSX, and NWZA, Figure 7 shows that the daily maximum temperature occurs around the time when the tidal current runs parallel to the bottom topography with the shallow areas to the right. This pattern can be explained by the fact that the tidal current close to the bottom at these sites turns anti-cyclonically almost always (Table A2) as illustrated in Figure 33. Thus the warmest bottom water occurs at the end of a period with the tidal current having an off-shelf component. Since the bottom temperature generally increases as we go towards shallower regions, this is just as expected.

For the site NWFG, we also see a clear indication of a tidal current effect (bin 1) on the bottom temperature, but the bottom water is coldest when we might have expected it to be warmest from the above argument. Partly, the reason for this may be that the near-bottom tidal current at this site is dominated by constituents – especially diurnal - that turn cyclonically rather than anticyclonically (Table A3). The tidal ellipses for the dominant constituents are, however, almost degenerated into straight lines at this site (Figure 33) and here at the sill of the Faroe Bank Channel, the isotherms descend in the direction of the mean flow (towards 305°). When the tidal current goes in the same direction, this should lead to lower bottom temperature, which is what Figure 7 shows.

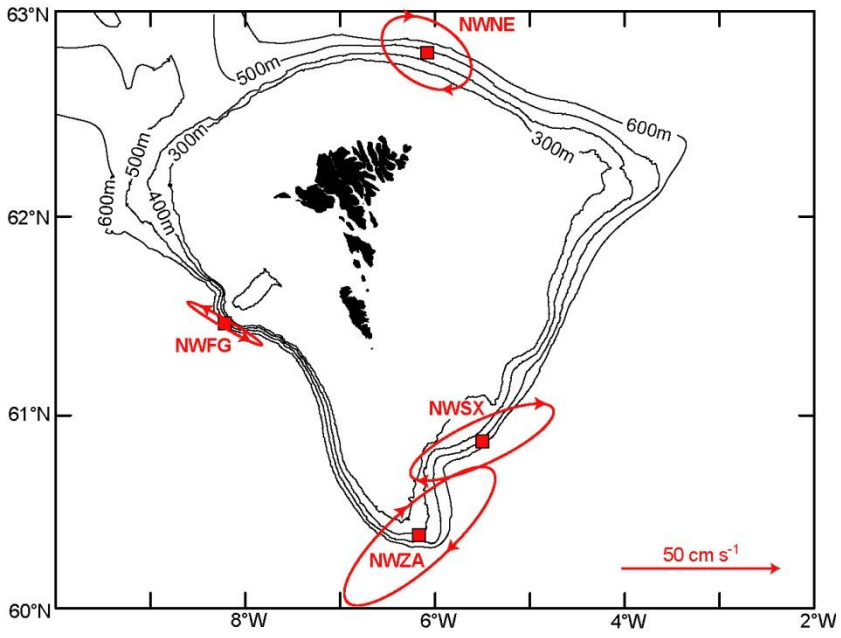

Figure 33. Tidal ellipses for the deepest bin (bin 1) from one deployment at each of the ADCP sites in the Transitional domain. For sites NWNE, NWSX, and NWZA, M2 was by far the dominant constituent (Table A2) and the ellipses are for that constituent. For site NWFG, all the tidal constituents were weak with the three diurnal constituents K1, O1, and P1 being almost equally dominant and the ellipse represents the sum of these three constituents.

6.3.2 The Transitional domain on the Iceland-Faroe Ridge

The Iceland-Faroe Ridge may be seen as an extension of the Faroe Plateau towards Iceland. The deepest passage across the ridge is slightly less than 500m deep and is located in the southeasternmost part of the ridge where it is connected to the Faroe Plateau (Figure 25). The near-surface regions above the ridge are dominated by warm Atlantic Water carried by the North Atlantic Current towards the Norwegian Sea (Figure 2a). This warm water may sometimes extend all the way to the bottom at least in some areas of the ridge but the near-bottom regions on the top of the ridge are also strongly affected by the cold IFR-overflow (Figure 2b) crossing from the Norwegian Sea into the Iceland Basin.

This interplay between warm and cold water leads to highly variable bottom temperatures on the Iceland-Faroe Ridge (IFR) as indicated by the values in Table 1 for the three IFR mooring sites (IFRA, IFRB, and IFRC) on the ridge. The

variability is further illustrated in the top panels of Figure 34, which show histograms of bottom temperature at these three sites. The most variable of these sites is IFRA, which also is the site with the highest standard deviation in Table 1. For this site, the bottom temperature was more than 1°C different from its average 72% of the time and more than 2°C different 42% of the time.

In addition to the high temporal variability, Figure 34 also demonstrates a high spatial variability. Although the three sites are located close to one another (Figure 31) and have almost identical bottom depths, there are substantial differences both in the average bottom temperature and its variability. Most likely, the local bottom topography affects the flow field across the ridge and the relative influences of the warm and the cold water masses at each location.

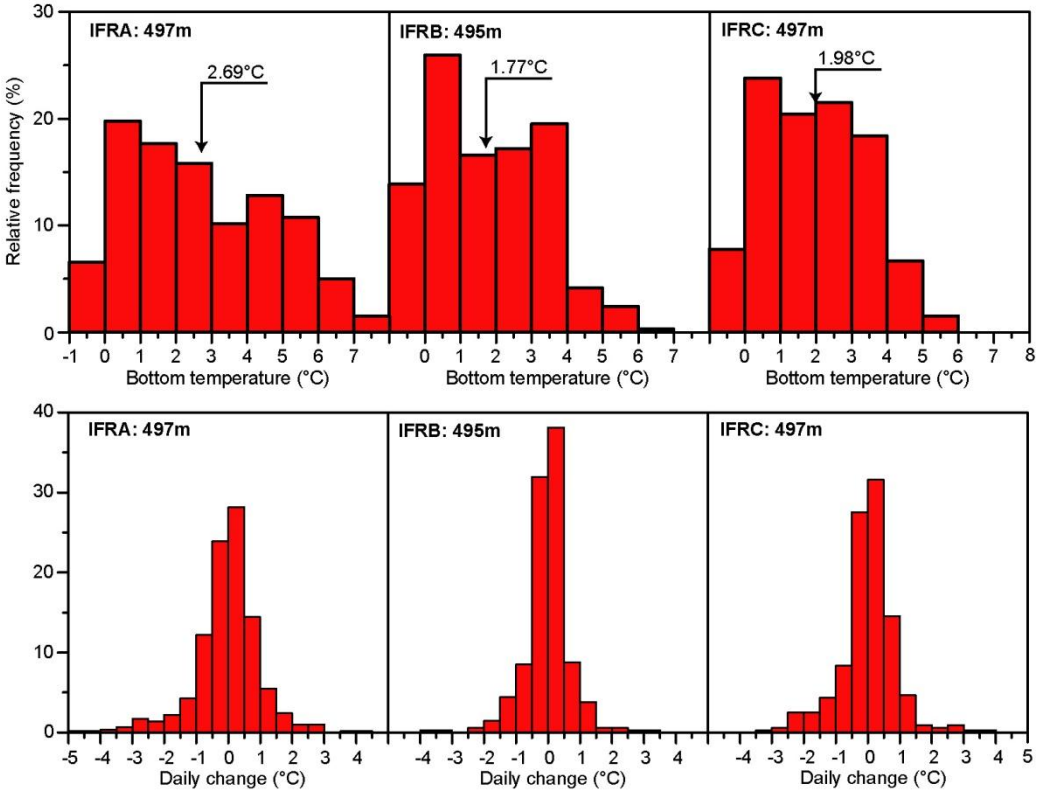

Figure 34. Bottom temperature variability at mooring sites on the Iceland-Faroe Ridge (for location, see Figure 31). Top panels show relative frequency (histogram) of bottom temperature at each site with the average temperature indicated by the arrow. Bottom panels show relative frequency (histogram) of the daily averaged temperature change from one day to the next.

The time series of bottom temperature on the Iceland-Faroe Ridge are too short to give any information on long-term variations and they do not indicate any consistent seasonal variation (Figure 6). On shorter time scales, the lower panels in Figure 34 show histograms of the change in bottom temperature from one day to another at the three IFR sites and again we see that considerable changes may occur on short time scales. At site IFRA, day-to-day temperature changes of more than ±1°C occurred 22% of the time. In Figure 7 there is an indication of increased bottom temperature at the three IFR mooring sites when the tidal current close to the bottom is directed towards the Norwegian Sea indicating stronger influence of Atlantic Water, as might be expected. The indication is, however, not very convincing and the correlation coefficients for these sites in Table 2 are low.

All of our mooring sites on the Iceland-Faroe Ridge are on its southwestern side, but close to the crest of the ridge. In Figure 27, the Transitional domain has been drawn all the way from east of the crest down to the 1000m isobath (the deep limit of this study). This is mainly based on the Seaglider data reported in Sect. 5 (Beaird et al., 2013). As illustrated in Figure 22 and Figure 24, the whole southwestern flank of the ridge has highly variable bottom temperatures with average values close to 3°C. In the region between 62°N and 63°N, there does not appear to be any systematic depth dependence of the bottom temperature between 500m and 1000m bottom depth (Figure 24), but north of 63°N, the coldest component is observed less frequently (Figure 22).

6.3.3 The Transitional domain on the Faroe Bank

On the Faroe Bank, the transitional domain covers a relatively narrow region where the Atlantic Water comes into contact with Deep Water on its way towards and past the overflow regions on the Wyville Thomson Ridge and in the Faroe Bank Channel. An instructive data set in this area is from CTD section V, which is located a short distance southeast of the sill of the Faroe Bank Channel (Figure 11), and Figure 35 illustrates the temperature variability on the deepest standard station, V06, on this section. As indicated in Figure 16a, a certain isotherm will normally hit the bottom on the Faroe Bank slope at a somewhat greater depth than on station V06, but the variability of the bottom temperature ought to be fairly similar to the variability on the station.

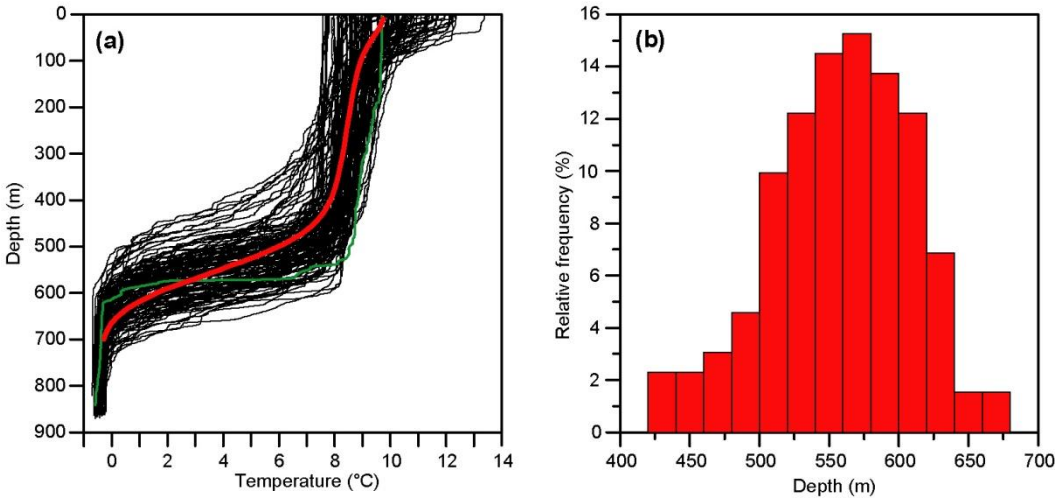

Figure 35. Temperature variations on standard station V06 (Figure 16) on section V (Figure 11) in the period 1988 - 2017. **(a)** Individual temperature profiles from 131 occupations of the station (black traces) and the average profile (thick red line). The green trace illustrates an individual profile with exceptionally sharp thermocline. **(b)** Frequency distribution (histogram) of the depth of the 3°C isotherm.

As indicated in Table 3, individual isotherms are located at considerably greater depth in the Transitional domain on Faroe Bank as compared to the Faroe Plateau, but they typically vary in depth by around ±100m (Figure 35b). The isotherms also tend to be closer in depth to one another on the Faroe Bank than on the Faroe Plateau. Thus, the depth difference between the 5°C isotherm and the 2°C isotherm where section V hits the bottom of the Faroe Bank was only 51m on average compared to 78m where section N hits bottom on the Faroe Plateau (Table 3). On the average temperature profile for station V06 (red line in Figure 35a), this depth difference was 65m. For all the 131 CTD profiles available, it never exceeded 112m and on one extreme occasion (green trace in Figure 35a), the temperature decreased from 5°C to 2°C within a 2m depth increase. This is consistent with the high standard deviations for station V06 at depths between 500m and 600m in Table 4.

A short distance northwest of section V, an Aanderaa current meter was deployed twice at a location on the Faroe Bank slope in the sill region in 2002 and 2003. The current meter was located 5m above the bottom and ought to measure bottom temperature accurately during the 142 days, which was the total duration of the two deployments. A histogram of bottom temperature at this site (Figure 36a) shows a bimodal distribution indicating that the bottom water at this site changes between almost pure Atlantic Water and almost pure Deep Water with only limited occurrence of mixtures between the two water masses.

The average temperature at this site, 4.68°C, is much higher than at the same depth farther southeast where section V intersects the bottom (Table 3). Partly, this may be due to a high uncertainty of the average value due to the short total period of the two deployments but, also, the isotherms are expected to deepen on the order of 100m as we approach the sill of the Faroe Bank Channel, as previously argued in Eq. (1).

The sharp thermocline in the Faroe Bank Channel (Figure 35a) and the bimodal bottom temperature distribution (Figure 36a) indicate that the changes in bottom temperature might occur quite rapidly as the thermocline moves up and down. This is indeed the case as demonstrated by Figure 36b, which shows the relative distribution of temperature changes from one hour to the next from the Aanderaa moorings. There changes of more than ±1°C within an hour occurred 26% of the time.

On the eastern flank of the Faroe Bank, the isotherms in general tend to deepen as we move northwestwards towards the sill of the Faroe Bank Channel and we also expect them to continue deepening after passing the sill as the FBC-

overflow descends towards deeper levels. This is also the impression from the Seaglider observations (Figure 26) and when we reach section W, the transitional domain has apparently descended below the 1000m isobath (Figure 17 and Table 4).

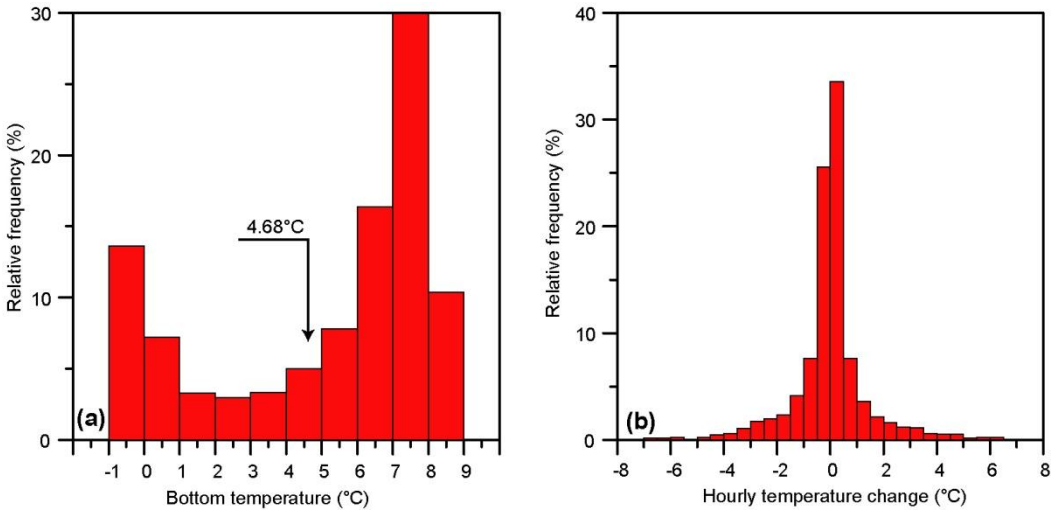

Figure 36. Bottom temperature at 650m depth at position 61.3777°N, 8.3281°W measured by Aanderaa current meters. **(a)** Relative frequency (histogram) of bottom temperature. The arrow indicates the average bottom temperature. **(b)** Relative frequency of change in bottom temperature from one hour to the next.

7 Sound speed correction of bottom depth

Determination of bottom depth by echo-sounder is based on measuring the time (Δt) that a sound pulse, transmitted from the surface, uses to return back to the surface after being reflected by the bottom. If the average sound speed for the whole water column is c_A, then the correct bottom depth D_C is given by: $D_C = ½ \cdot \Delta t \cdot c_A$. Usually, c_A is not known a priori and so a fixed sound speed c_E is assumed. For a CTD station, the correct value for c_A may be calculated from the CTD profile, which allows the correct bottom depth to be derived from the depth (D_E) reported by the echo-sounder: $D_C = D_E \cdot c_A/c_E$.

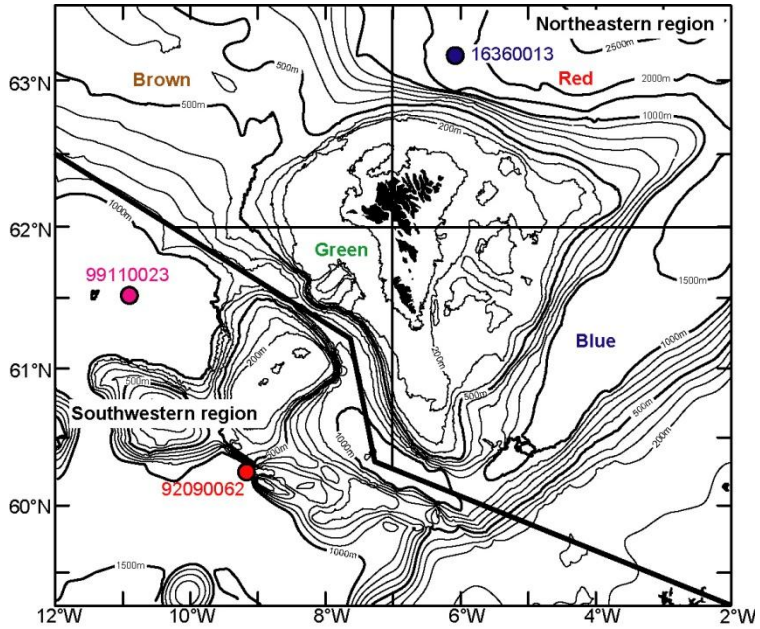

Figure 37. Locations of the three CTD stations used as examples to illustrate the variable sound speed profiles in Figure 38 are indicated by circles. Thick black line shows the separation between the Faroe Plateau and the Southwestern region. Thin black lines show the separation of the Faroe Plateau into four subregions with colours referring to Figure 39.

Faroese hydrographic data have been collected with research vessels that have had echo-sounders with c_E = 1500 m/s. Sound speed generally increases with temperature, salinity, and pressure (depth), but the effect of salinity change is only around 1 m/s. Thus, the depth variation of sound speed becomes a combination of the decreasing temperature and the increasing pressure. This leads to different sound speed profiles in the Southwestern region compared to the area around the Faroe Plateau as illustrated by three examples in Figure 38.

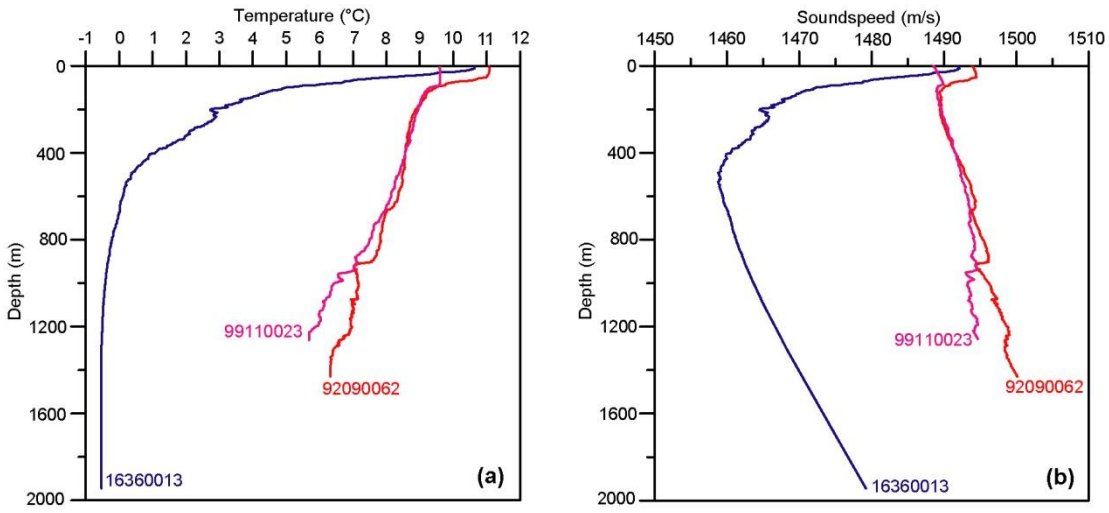

Figure 38. Profiles of temperature **(a)** and sound speed **(b)** for the three CTD stations shown by coloured circles in Figure 37.

Generally, the sound speed is less than 1500 m/s almost everywhere in Faroese waters and we should expect $c_A/c_E < 1$, i.e.: $D_C < D_E$. To correct echo-sounder depth, we therefore need to subtract a value $\delta D = D_E - D_C$. Since δD usually increases with depth, it is useful to consider the relative depth correction $\delta D / D_E$ and that is what is shown in Figure 39. In this figure, each dot represents the relative depth correction for one CTD station. Since the CTD normally does not go all the way to bottom, it is necessary to extrapolate, which is done by extending the deepest observation downwards. For stations shallower than 800 m, the restriction, that the deepest CTD observation should be no more than 30 m from the bottom and that the temperature gradient close to bottom not be too high (Sect. 3), should ensure that associated errors introduced by the extrapolation are small. For deeper stations, we require that the CTD reaches at least down to 750 m. Around the Faroe Plateau (Figure 39b), this should ensure that the temperature is close to its coldest value. In the Southwestern region, we require additionally that the CTD reaches at least 90% of the echo-sounder depth.

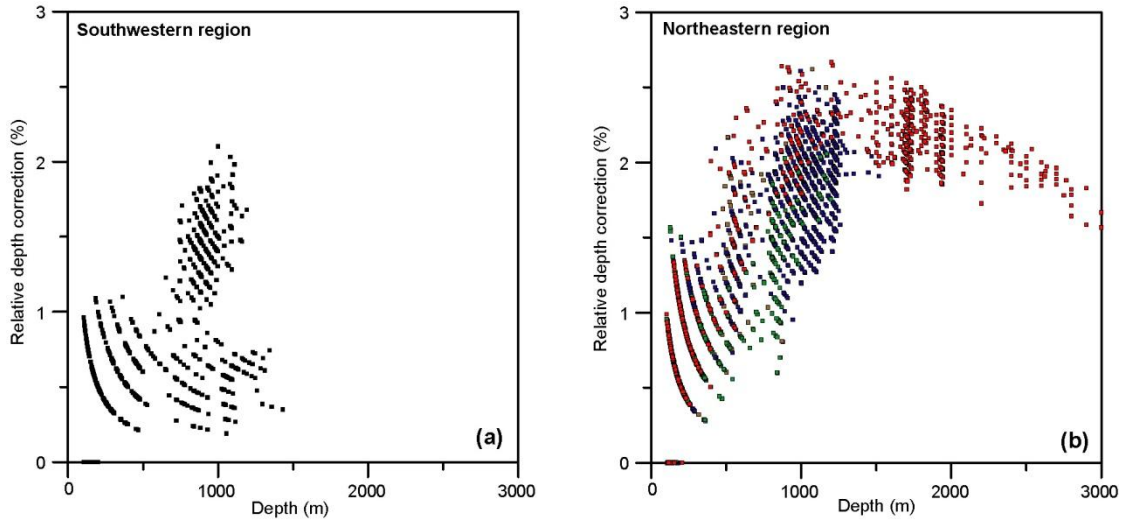

Figure 39. Percentage depth correction to subtract from echo-sounder depth (assuming 1500 m/s) for the Southwestern region **(a)** and for four subregions in the Northeastern region **(b)** with colours indicated in Figure 37.

As seen in Figure 39, there is considerable scatter in the relative depth correction, which is mainly due to variation in temperature profiles. The highest relative corrections are found at depths around 1000 m in the cold regions northeast of the Faroes (red dots in Figure 39b). In the Southwestern region, areas that are affected by the cold overflow may also exhibit fairly high relative corrections, but the regions that remain fairly warm to large depths have smaller values (Figure 39a).

References

Beaird, N. L., Rhines, P. B., and Eriksen, C. C.: Overflow waters at the Iceland-Faroe Ridge observed in multiyear Seaglider surveys, J. Phys. Oceanogr., 43, 2334–2351, doi:10.1175/JPO-D-13-029.1, 2013.

Geyer, F., Østerhus, S., Hansen, B., and Quadfasel, D.: Observations of highly regular oscillations in the overflow plume downstream of the Faroe Bank Channel, J. Geophys. Res., 111, C12020, doi:10.1029/2006JC003693, 2006.

Hansen, B. and Østerhus, S.: Faroe Bank Channel overflow 1995-2005, Prog. Oceanogr., 75, 817-856, doi:10.1016/j.pocean.2007.09.004, 2007.

Hansen, B., Poulsen, T., Húsgarð Larsen, K. M., Hátún, H., Østerhus, S., Darelius, E., Berx, B., Quadfasel, D., and Jochumsen, K.: Atlantic water flow through the Faroese Channels, Ocean Sci., 13, 873-888, https://doi.org/10.5194/os-13-873-2017, 2017.

Larsen, K. M. H., Hansen, B., and Svendsen, H.: Faroe Shelf Water, Cont. Shelf Res., 28, 1754-1768, doi:10.1016/j.csr.2008.04.006, 2008.

Larsen, K.M.H., Hansen, B., and Svendsen, H.: The Faroe Shelf Front: Properties and exchange. J. Mar. Syst. 78, 9–17. doi:10.1016/j.jmarsys.2009.02.003, 2009.

Larsen, K. M. H., Hátún, H., Hansen, B., and Kristiansen, R.: Atlantic water in the Faroe area: sources and variability, ICES J. Mar. Sci., 69, 802-808, doi:10.1093/icesjms/fss028, 2012.

Pyper, B. J. and Peterman, R. M.: Comparison of methods to account for autocorrelation in correlation analyses of fish data, Can. J. Fish. Aquat. Sci., 55, 2127-2140, doi:10.1139/f98-104, 1998.

Westerberg, H.: Benthic temperature in the Faroe area, Department of oceanography, University of Gothenburg, Sweden, Report no 51, 1990.

Appendix A

Table A1. List of records from self-recording Instruments deployed on or very close to (< 10m) the bottom. For ADCP deployments, "Bin1" lists the depth of the first bin. The next two columns show bin number (Top) and depth (Topd) for the uppermost bin for which 80% of data are good. The last four columns list the characteristics of the tidal ellipse for the M2 tidal current of bin1 with major and minor semi-axes in cm s^{-1}, inclination from North, and sense of rotation (R = A: Anticyclonic, R = C: Cyclonic). The first one or two letters of the instruments indicate instrument type: "A" is for ADCP, "BT" for bottom temperature logger, "M" is for SeaBird Microcat, "R" is for Aanderaa RCM.

Deploym.	Inst	Period	Latitude	Longitude	Botm	Bin1	Top	Topd	Major	Minor	Incl	R
NT021510	BT02	20151015-20170831	62°39.920'N	6°04.960'W	185							
WT011510	BT03	20151017-20170902	61°30.000'N	7°34.900'W	243							
NWSA9511	A1278	19951110-19960527	61°00.069'N	5°50.027'W	298	283	20	93	21.2	3.1	63	A
NWSA9606	A1278	19960614-19970523	60°59.818'N	5°50.459'W	295	278	20	88	21.5	3.4	66	A
NWSA9811	A1279	19981106-19990612	61°00.137'N	5°50.612'W	295	278	19	98	21.8	3.7	64	A
NWSA9907	A1244	19990706-20000620	61°00.000'N	5°51.400'W	293	276	18	106	22.5	4.0	63	A
NWNA9601	A1244	19960124-19960526	62°42.370'N	6°05.310'W	302	287	17	127	13.4	6.1	102	A
NWNA9606	A1244	19960616-19970522	62°41.928'N	6°04.665'W	292	275	19	95	14.1	6.9	117	A
NWNA9706	A1244	19970614-19980609	62°42.315'N	6°05.170'W	300	283	21	83	14.3	7.5	118	A
NWNA9807	A1244	19980707-19990702	62°42.178'N	6°05.043'W	297	280	20	90	15.0	8.0	108	A
NWNA9907	A1279	19990702-20000616	62°41.947'N	6°03.887'W	295	278	18	108	14.3	7.3	119	A
NWNA0007	A1279	20000707-20010616	62°42.048'N	6°04.456'W	297	280	20	90				
NWNA0107	A1279	20010706-20020614	62°42.100'N	6°04.100'W	298	281	16	131	14.3	7.6	112	A
NWNA0207	A1279	20020705-20030614	62°42.200'N	6°04.330'W	301	284	18	114	13.7	7.2	113	A
NWNA0307	A1279	20030704-20040611	62°41.992'N	6°04.865'W	294	277	19	97	13.9	6.9	113	A
NWNA0407	A1279	20040702-20050520	62°42.020'N	6°05.072'W	293	276	20	86	14.0	7.3	117	A
NWNA0506	A1279	20050611-20060523	62°41.945'N	6°04.312'W	303	286	19	106	14.0	7.1	110	A
NWNA0606	A1279	20060609-20070518	62°42.307'N	6°04.697'W	304	287	20	97	14.8	7.8	116	A
NWNA0706	A1279	20070608-20080518	62°42.207'N	6°04.712'W	303	286	18	116	14.0	7.0	116	A
NWNA0806	A1279	20080605-20090515	62°41.996'N	6°05.114'W	296	279	18	109	14.1	7.4	116	A
NWNA0906	A1279	20090605-20100514	62°41.983'N	6°05.115'W	301	284	20	94	14.1	7.0	122	A
NWNA1006	A1279	20100604-20110520	62°42.080'N	6°04.800'W	298	281	18	111	14.2	7.4	114	A
NWNA1106	A1279	20110610-20120520	62°42.170'N	6°05.078'W	298	281	17	121	13.9	7.0	116	A
NWNA1206	A1279	20120607-20130517	62°42.200'N	6°04.900'W	300	283	19	103	14.0	7.3	120	A
NWNA1306	A1279	20130609-20140515	62°42.039'N	6°04.610'W	300	283	18	113	13.7	7.2	116	A
NWNA1406	A1279	20140605-20150525	62°42.153'N	6°05.053'W	300	283	18	113	14.1	7.1	115	A
NWZA1106	A3368	20110611-20120518	60°23.403'N	6°09.590'W	416	397	35	57	32.0	10.6	47	A
NWZA1306	A3368	20130607-20140517	60°23.300'N	6°09.600'W	417	397	35	57	30.6	9.5	48	A
NWNE0007	A1244	20000706-20010616	62°47.490'N	6°05.100'W	456	424	11	174				
NWNE0107	A1244	20010706-20031230	62°47.537'N	6°04.240'W	447							
NWNE0407	A1244	20040702-20050520	62°47.510'N	6°05.352'W	455	432	12	157	14.9	9.3	129	A
NWNE0506	A1244	20050611-20060523	62°47.440'N	6°04.422'W	456	424	12	149	14.3	8.5	125	A
NWNE0606	A1244	20060609-20070518	62°47.786'N	6°04.577'W	462	431	12	156	16.7	11.6	120	A
NWNE0706	A1244	20070608-20080518	62°47.421'N	6°05.059'W	450	418	11	168	16.2	10.4	124	A
NWNE0806	A1244	20080606-20090515	62°47.636'N	6°04.905'W	457	425	12	150	14.6	9.0	133	A
NWNE0906	A1244	20090605-20100514	62°47.628'N	6°04.914'W	455	423	12	148	15.2	9.6	122	A
NWNE1006	A1244	20100604-20110520	62°47.590'N	6°04.980'W	456	424	12	149	13.6	7.8	124	A
NWNE1410	BT01	20141018-20150905	62°47.700'N	6°04.900'W	448							
IFRA0307	M981	20030704-20040611	62°37.960´N	8°28.385´W	496							
IFRA0409	A5516	20040906-20050524	62°38.100'N	8°27.200'W	498	480	43	60	25.3	5.3	68	A
IFRB0307	A3368	20030704-20040611	62°51.668'N	8°35.360'W	495	475	43	55	17.9	0.3	57	A
IFRC0407	A3368	20040703-20050524	62°45.805'N	9°42.697'W	497	479	43	59	19.3	4.8	53	A
NWSX0906	M984	20090606-20100517	60°51.500´N	5°29.700´W	552							
NWSX1006	A3368	20100604-20110521	60°51.510'N	5°30.120'W	549	530	47	70	24.6	6.8	65	A
NWSX1206	A3368	20120609-20130519	60°51.670'N	5°29.750'W	546	526	45	86	24.5	7.2	72	A
NWFG0805	A3368	20080516-20090516	61°28.260'N	8°13.251'W	561	542	46	92	2.3	1.4	134	A
NWFB0107	A1642	20010708-20020616	61°24.923'N	8°16.965'W	814	772	16	397	3.1	2.2	71	A
NWFB0207	A1642	20020707-20030616	61°24.942'N	8°16.870'W	812	770	17	370	3.4	2.0	88	A
NWFB0307	A1642	20030705-20040612	61°24.890'N	8°16.930'W	813	771	17	371	2.6	1.7	99	A
NWFB0407	A1642	20040703-20050523	61°24.974'N	8°16.906'W	812	770	17	370	2.3	1.6	97	A
NWFB0506	A1642	20050611-20060524	61°24.897'N	8°17.097'W	817	775	22	250	2.3	1.8	88	A
NWFB0606	A1642	20060612-20070519	61°25.051'N	8°17.244'W	812	771	18	346	2.6	2.1	97	A
NWFB0706	A1642	20070609-20080516	61°25.038'N	8°16.983'W	812	771	17	371	2.9	2.1	91	A
NWFB0806	A1642	20080606-20090605	61°25.002'N	8°16.866'W	812	771	16	396	2.7	2.1	95	A
NWFB0906	A1642	20090607-20100515	61°25.000'N	8°16.800'W	812	771	16	396	3.0	2.4	101	A
NWFB1006	A1642	20100605-20110523	61°25.000'N	8°17.000'W	814	773	16	398	3.0	1.9	83	A
NWFB1106	A1642	20110612-20120522	61°24.988'N	8°16.975'W	808	767	16	392	2.8	2.0	101	A
NWFB1209	A3486	20120930-20130516	61°24.870'N	8°17.241'W	822	796	52	286	0.6	0.2	133	C
NWFB1306	A1577	20130607-20140516	61°24.951'N	8°16.987'W	814	771	19	321	2.7	2.1	99	A
NWFB1406	A1577	20140609-20150524	61°24.951'N	8°17.000'W	809	767	19	317	2.9	2.0	105	A
NWFB1506	A1285	20150613-20160521	61°25.000'N	8°16.900'W	812	770	21	270	2.3	2.1	123	A
NWFB1606	A1577	20160610-20170518	61°25.044'N	8°16.937'W	811	769	19	319				
FOIC0107	R9718	20010707-20020616	60°38.629'N	5°04.489'W	910							
FOIB0107	R9721	20010707-20020616	60°25.512'N	5°00.424'W	932							
FOIA0107	A1285	20010707-20020616	60°25.248'N	5°18.735'W	986	944	26	319	19.5	3.3	54	C

Table A2. Major semi-axis and sense of rotation (C = Cyclonic, A = Anticyclonic) for the 9 most important tidal constituents for bin 1 of each ADCP deployment. The last column indicates "Percentage anticyclonic" defined as the sum of anticyclonic semi-axes divided by the total sum of semi-axes multiplied by 100.

Deploym.	Q1	O1	P1	K1	N2	M2	L2	S2	K2	%A
NWSA9511	1.3 A	3.8 A	1.1 A	2.2 A	3.9 A	21.2 A	0.9 A	7.7 A	1.9 A	100
NWSA9606	1.2 A	4.1 A	0.8 A	3.1 A	4.7 A	21.5 A	0.4 A	7.6 A	1.9 A	100
NWSA9811	1.3 A	4.0 A	1.1 A	2.6 A	4.2 A	21.8 A	0.5 A	7.8 A	2.3 A	100
NWSA9907	1.0 A	3.9 A	1.1 A	2.8 A	4.6 A	22.5 A	0.5 A	7.5 A	2.0 A	100
NWNA9601	1.3 A	2.3 A	1.4 A	4.3 A	2.3 A	13.4 A	0.5 A	4.3 A	1.2 A	100
NWNA9606	1.4 A	2.5 A	0.4 C	3.6 A	2.4 A	14.1 A	0.7 A	5.5 A	1.6 A	99
NWNA9706	1.4 A	2.4 A	0.5 A	3.1 A	3.1 A	14.3 A	1.3 A	4.9 A	1.4 A	100
NWNA9807	0.9 A	2.4 A	0.5 C	4.1 A	2.6 A	15.0 A	1.1 A	5.1 A	0.9 A	98
NWNA9907	1.0 A	2.8 A	0.4 A	3.0 A	2.6 A	14.3 A	0.5 A	5.0 A	1.4 A	100
NWNA0107	0.9 A	2.2 A	0.3 C	3.1 A	2.6 A	14.3 A	1.0 A	4.9 A	1.5 A	99
NWNA0207	1.0 A	2.5 A	0.9 A	3.0 A	2.8 A	13.7 A	1.2 A	4.8 A	1.6 A	100
NWNA0307	1.4 A	2.5 A	0.7 A	3.5 A	2.8 A	13.9 A	0.6 A	5.5 A	1.3 A	100
NWNA0407	1.4 A	2.2 A	0.5 C	3.3 A	3.0 A	14.0 A	0.1 A	5.1 A	1.2 A	98
NWNA0506	0.9 A	1.9 A	0.7 A	3.1 A	2.6 A	14.0 A	1.1 A	4.9 A	1.2 A	100
NWNA0606	1.1 A	2.3 A	0.8 A	3.0 A	3.2 A	14.8 A	1.2 A	5.3 A	1.7 A	100
NWNA0706	0.8 A	2.3 A	0.6 A	3.1 A	3.0 A	14.0 A	0.7 A	4.8 A	1.5 A	100
NWNA0806	0.7 A	2.0 A	1.1 A	2.6 A	2.9 A	14.1 A	0.5 A	4.8 A	1.7 A	100
NWNA0906	0.7 A	2.2 A	0.3 A	3.2 A	3.1 A	14.1 A	0.6 A	4.9 A	1.9 A	100
NWNA1006	1.4 A	2.4 A	0.7 A	3.1 A	2.4 A	14.2 A	1.0 A	4.6 A	1.9 A	100
NWNA1106	1.2 A	2.6 A	0.4 C	3.2 A	2.7 A	13.9 A	1.0 A	4.3 A	1.3 A	99
NWNA1206	1.5 A	2.6 A	0.3 A	3.0 A	3.1 A	14.0 A	1.1 A	4.7 A	2.1 A	100
NWNA1306	1.1 A	2.3 A	0.5 A	3.2 A	2.8 A	13.7 A	0.4 A	5.0 A	2.1 A	100
NWNA1406	1.2 A	2.6 A	0.6 C	2.8 A	2.5 A	14.1 A	1.0 A	5.1 A	1.9 A	98
NWZA1106	0.8 A	1.6 A	0.5 A	1.3 C	5.3 A	32.0 A	2.6 A	12.4 A	4.6 A	98
NWZA1306	0.6 C	1.5 C	0.4 C	1.2 A	7.0 A	30.6 A	0.7 A	12.8 A	4.1 A	96
NWNE0407	0.8 A	2.3 A	0.8 A	2.2 A	3.1 A	14.9 A	0.6 A	6.7 A	1.3 A	100
NWNE0506	1.3 A	1.7 A	0.7 A	1.9 A	3.2 A	14.3 A	1.2 A	5.4 A	1.9 A	100
NWNE0606	0.8 A	2.0 A	1.0 A	2.5 A	3.2 A	16.7 A	2.4 A	6.4 A	1.9 A	100
NWNE0706	1.0 A	2.0 A	0.3 A	1.9 A	3.5 A	16.2 A	1.0 A	5.4 A	2.0 A	100
NWNE0806	0.5 A	2.2 A	0.3 A	2.1 A	2.0 A	14.6 A	1.3 A	7.5 A	1.9 A	100
NWNE0906	1.2 A	2.2 A	0.6 A	2.1 A	2.0 A	15.2 A	0.3 C	5.7 A	1.4 A	99
NWNE1006	0.4 A	1.6 A	0.9 A	2.0 A	2.4 A	13.6 A	1.8 A	4.9 A	2.0 A	100
IFRA0409	1.7 A	2.8 A	1.0 A	2.7 A	4.4 A	25.3 A	0.9 A	9.8 A	3.2 A	100
IFRB0307	1.8 A	2.9 A	0.6 A	2.7 A	3.4 C	17.9 A	0.6 A	7.0 A	2.5 A	91
IFRC0407	1.7 A	2.6 A	0.8 A	2.9 A	4.0 A	19.3 A	0.4 A	7.0 A	1.5 A	100
NWSX1006	2.2 C	7.1 C	1.5 C	5.5 A	4.5 A	24.6 A	1.5 A	8.4 A	1.9 C	78
NWSX1206	1.7 C	7.6 C	2.0 C	5.1 A	5.4 A	24.5 A	0.5 C	9.2 A	3.2 A	80
NWFG0805	1.7 C	4.8 C	3.2 C	5.4 C	0.3 C	2.3 A	0.5 C	1.8 C	0.4 A	13
NWFB0107	0.7 C	2.4 C	1.1 C	2.2 C	0.8 A	3.1 A	0.3 A	1.3 A	0.6 A	49
NWFB0207	0.7 C	2.1 C	0.9 C	2.1 A	0.8 A	3.4 A	0.5 A	1.3 A	0.3 A	69
NWFB0307	0.5 A	2.9 C	1.2 A	2.4 C	0.8 A	2.6 A	0.3 C	1.5 A	0.7 A	57
NWFB0407	0.7 C	2.3 C	1.3 A	1.9 A	0.4 C	2.3 A	0.3 A	1.0 A	0.5 A	68
NWFB0506	0.7 A	1.8 A	0.9 A	2.2 A	0.6 A	2.3 A	0.3 A	1.2 A	0.5 A	100
NWFB0606	0.6 A	1.8 C	0.9 A	1.8 C	1.0 A	2.6 A	0.7 A	0.9 A	0.5 A	67
NWFB0706	0.8 A	1.6 C	1.0 A	1.7 A	1.0 A	2.9 A	0.2 C	1.0 A	0.5 A	83
NWFB0806	0.3 C	2.3 A	1.1 A	2.0 A	0.7 A	2.7 A	0.3 A	1.2 A	0.5 A	97
NWFB0906	0.6 A	1.9 A	1.0 C	1.5 A	0.8 A	3.0 A	0.2 A	1.4 A	0.7 A	91
NWFB1006	0.7 C	1.8 A	1.3 A	2.0 A	0.9 A	3.0 A	0.8 A	1.4 A	0.6 A	94
NWFB1106	0.8 C	1.8 C	1.0 A	1.9 A	0.7 C	2.8 A	0.8 A	1.3 A	0.5 A	72
NWFB1209	0.2 A	0.3 A	0.9 A	1.0 A	0.4 A	0.6 C	0.2 C	0.7 A	0.5 A	83
NWFB1306	0.5 A	2.1 A	0.9 A	1.7 A	0.7 A	2.7 A	0.6 A	1.3 A	0.2 A	100
NWFB1406	0.6 A	1.8 A	0.9 A	2.1 A	1.0 A	2.9 A	0.3 C	0.9 A	0.3 C	94
NWFB1506	0.6 C	2.0 A	0.8 A	1.9 C	0.7 A	2.3 A	0.2 C	1.1 A	0.6 A	74
FOIA0107	0.8 C	1.8 C	0.3 C	1.2 C	4.1 C	19.5 C	1.3 A	7.6 C	2.2 C	3

Table A3. Major semi-axis and sense of rotation (C = Cyclonic, A = Anticyclonic) for the 9 most important tidal constituents for the deepest 50 bins of ADCP deployment NWFG0805. The last column indicates “Percentage anticyclonic” defined as the sum of anticyclonic semi-axes divided by the total sum of semi-axes multiplied by 100.

Bin	Depth	Q1	O1	P1	K1	N2	M2	L2	S2	K2	%A
1	542	1.7 C	4.8 C	3.2 C	5.4 C	0.3 C	2.3 A	0.5 C	1.8 C	0.4 A	13
2	532	1.6 C	4.9 C	3.3 C	5.4 C	0.3 C	2.0 A	0.4 C	1.6 C	0.5 A	13
3	522	1.6 C	4.8 C	3.2 C	5.3 A	0.3 A	1.6 A	0.3 C	1.3 C	0.5 A	41
4	512	1.5 C	4.6 C	2.9 C	4.7 A	0.3 A	1.3 A	0.2 C	1.5 C	0.5 A	39
5	502	1.4 C	4.3 C	2.8 C	4.3 A	0.3 C	1.4 C	0.4 A	1.6 C	0.8 A	32
6	492	1.3 C	4.0 C	2.4 C	3.8 A	0.5 C	1.9 C	0.4 A	2.0 C	0.9 A	30
7	482	1.0 C	3.6 C	2.2 C	3.2 C	0.7 C	2.6 C	0.3 A	2.2 C	1.1 A	8
8	472	0.8 C	3.2 C	2.0 C	2.6 C	0.9 C	3.5 C	0.3 A	2.3 C	1.2 A	9
9	462	0.6 C	2.9 C	1.7 C	2.3 C	1.0 C	4.2 A	0.3 A	2.5 A	1.3 C	42
10	452	0.5 C	2.5 C	1.5 C	2.0 C	1.2 A	4.9 A	0.3 A	2.6 A	1.3 A	61
11	442	0.5 C	2.1 C	1.3 C	1.8 C	1.4 A	5.7 A	0.3 A	2.7 A	1.2 A	66
12	432	0.6 C	1.8 C	1.0 C	1.6 C	1.5 A	6.3 A	0.1 C	2.9 A	1.1 A	70
13	422	0.5 C	1.5 C	0.9 C	1.7 C	1.7 A	7.0 A	0.3 C	2.9 A	0.9 A	72
14	412	0.4 C	1.4 C	0.9 C	1.7 C	1.7 A	7.7 A	0.4 A	3.1 A	0.9 A	76
15	402	0.4 C	1.5 C	0.9 C	1.6 C	1.8 A	8.5 A	0.4 A	3.2 A	0.9 A	77
16	392	0.5 A	1.4 C	0.9 C	1.5 C	1.9 A	9.3 A	0.4 A	3.3 A	1.1 A	81
17	382	0.6 A	1.4 C	1.0 C	1.4 C	2.0 A	10.0 A	0.2 A	3.5 A	1.1 A	82
18	372	0.7 A	1.4 C	0.9 C	1.2 C	2.1 A	10.5 A	0.2 A	3.7 A	1.1 A	84
19	362	0.7 A	1.5 C	0.9 C	1.1 C	2.1 A	11.0 A	0.2 A	3.9 A	1.1 A	84
20	352	0.7 A	1.5 C	0.8 C	1.1 C	2.2 A	11.5 A	0.3 A	4.0 A	1.2 A	85
21	342	0.8 A	1.7 A	0.9 C	1.1 C	2.3 A	11.8 A	0.4 A	4.0 A	1.2 A	92
22	332	0.6 A	1.6 A	0.8 C	1.1 C	2.3 A	12.1 A	0.4 A	4.0 A	1.2 A	92
23	322	0.6 A	1.6 A	0.8 C	1.1 C	2.3 A	12.3 A	0.4 A	4.0 A	1.1 A	92
24	312	0.6 A	1.6 A	0.9 C	1.0 C	2.2 A	12.5 A	0.4 A	4.1 A	1.2 A	92
25	302	0.5 A	1.6 A	1.1 C	1.0 C	2.3 A	12.8 A	0.4 A	4.2 A	1.1 A	92
26	292	0.5 A	1.6 A	1.0 C	1.1 C	2.2 A	12.8 A	0.4 A	4.2 A	1.2 A	92
27	282	0.5 A	1.7 C	1.0 C	1.0 C	2.1 A	12.9 A	0.4 A	4.2 A	1.2 A	85
28	272	0.4 A	1.7 C	0.9 C	1.0 C	2.1 A	13.0 A	0.5 A	4.2 A	1.3 A	86
29	262	0.5 A	1.7 C	0.8 C	1.1 C	2.0 A	13.1 A	0.5 A	4.2 A	1.3 A	86
30	252	0.5 A	1.7 C	0.8 C	1.3 C	2.1 A	13.0 A	0.5 A	4.3 A	1.4 A	85
31	242	0.5 A	1.6 C	0.6 C	1.2 C	2.1 A	13.2 A	0.5 A	4.3 A	1.5 A	87
32	232	0.5 A	1.7 C	0.6 C	1.3 C	2.1 A	13.2 A	0.5 A	4.3 A	1.4 A	86
33	222	0.5 A	1.8 C	0.6 C	1.3 C	2.0 A	13.3 A	0.4 A	4.2 A	1.5 A	86
34	212	0.6 A	1.8 C	0.6 C	1.4 C	1.9 A	13.4 A	0.4 A	4.2 A	1.4 A	85
35	202	0.7 A	1.7 A	0.8 C	1.3 C	1.8 A	13.6 A	0.4 A	4.3 A	1.4 A	92
36	192	0.7 C	1.7 A	0.9 C	1.3 C	1.9 A	13.7 A	0.3 A	4.4 A	1.4 A	89
37	182	0.6 A	1.9 A	0.9 C	1.4 C	2.0 A	13.8 A	0.4 A	4.5 A	1.5 A	91
38	172	0.6 C	2.0 A	1.0 C	1.3 C	2.0 A	13.9 A	0.5 A	4.7 A	1.7 A	90
39	162	0.6 C	2.0 A	0.9 C	1.4 C	2.1 A	14.1 A	0.4 A	4.8 A	1.7 A	90
40	152	0.6 A	2.0 A	1.0 C	1.3 C	2.1 A	14.2 A	0.6 A	4.8 A	1.7 A	92
41	142	0.6 C	2.0 A	1.0 C	1.3 C	2.4 A	14.3 A	0.7 A	5.0 A	1.8 A	90
42	132	0.6 A	2.0 A	1.1 C	1.3 A	2.4 A	14.5 A	0.8 A	5.0 A	1.9 A	96
43	122	0.6 A	2.0 A	1.2 C	1.3 A	2.5 A	14.4 A	1.0 A	4.9 A	1.8 A	96
44	112	0.6 A	2.1 A	1.3 C	1.4 A	2.8 A	14.7 A	1.0 A	4.8 A	2.1 A	96
45	102	0.5 A	1.9 A	1.4 C	1.4 A	2.9 A	14.9 A	0.9 A	4.8 A	2.0 A	95
46	92	0.5 A	2.0 A	1.3 C	1.3 A	3.3 A	14.9 A	1.1 A	4.7 A	2.1 A	96
47	82	0.7 A	1.8 A	1.1 C	1.5 A	3.6 A	15.3 A	1.0 A	4.7 A	2.3 A	97
48	72	0.6 A	2.0 A	1.3 C	1.2 C	3.6 A	14.9 A	0.8 A	4.6 A	2.1 A	92
49	62	0.9 A	2.1 A	1.1 C	1.3 A	3.6 A	15.5 A	0.7 A	4.5 A	2.1 A	97
50	52	0.9 A	2.0 A	1.2 A	1.7 C	3.8 A	15.9 A	0.8 A	4.5 A	1.8 A	95

Appendix B

Statistical significance

To estimate the statistical significance of correlation coefficients, we have used the "Modified Chelton method" recommended by Pyper and Peterman (1998) to correct for serial correlation in the data. Significance level is indicated by asterisks attached to the correlation coefficient. * indicates $p < 0.05$, ** indicates $p < 0.01$, *** indicates $p < 0.001$. All of these are two-tailed probabilities.

Iterative splitting of time series into seasonal and long-term variations

Several of the time series considered in this report may be seen as superpositions of slowly varying signals + seasonal signals + short-term variations. The seasonal variation generally has a roughly sinusoidal shape and a simple analysis may be made by regressing the time series on a sinusoidal seasonal variation where the phase lag is varied to give maximum correlation. The long-term variation may since be calculated as a running mean of deseasoned values.

In this analysis, the seasonal variation is, however, often contaminated by the long-term variation and vice versa. To overcome this, we may use a more refined iterative procedure. First, we fit a sinusoidal seasonal variation to the raw series. This seasonal signal is subtracted from the raw series to produce a deseasoned signal, which is averaged over 3 years. The 3-year running mean is subtracted from the raw series and the process repeated iteratively until it converges, which it does rapidly. In this way, we get a seasonal signal that is not so much contaminated by long-term variations and we get a time series of 3-year running mean, which is the average of all the deseasoned values within each 3-year period. This also allows us to calculate the standard error of each 3-year mean value.

P.O. Box 3051 · Nóatún 1
FO-110 Tórshavn
Faroe Islands

Tel +298 35 39 00
hav@hav.fo
www.hav.fo